PLOS Water

RESEARCH ARTICLE

Experimental investigation of magnetic ring fins with variable spacing in a hemispherical solar still: A 4E assessment

Abdekader S. Abdullah[1], Eyad Zaky[1], Suha A. Mohammed[2], Ismail Solmaz[3], Sengottain Shanmugan[4], Hamada Mohamed Abdelmotalib[5], Khaled Harby[6]*

1 Department of Mechanical Engineering, College of Engineering in Al-Kharj, Prince Sattam bin Abdulaziz University, Al-Kharj, Saudi Arabia, **2** Energy and Renewable Energies Technology Research Center, University of Technology, Baghdad city, Iraq, **3** Department of Mechanical Engineering, Faculty of Engineering, Ataturk University, Erzurum, Turkey, **4** Research Centre for Solar Energy, Department of Integrated Research and Discovery; Physics, Koneru, Guntur city, India, **5** Mechanical Power Engineering and Energy Department, Faculty of Engineering, Minia University, Minia, Egypt, **6** Department of Mechanical Engineering, College of Engineering, Taibah University, Al-Madinah Al-Munawarah, Saudi Arabia

* Khaledharby8@yahoo.com

Check for updates

OPEN ACCESS

Citation: Abdullah AS, Zaky E, Mohammed SA, Solmaz I, Shanmugan S, Abdelmotalib HM, et al. (2026) Experimental investigation of magnetic ring fins with variable spacing in a hemispherical solar still: A 4E assessment. PLOS Water 5(11): e0000568. https://doi.org/10.1371/journal.pwat.0000568

Editor: Prasenjit Chakraborty, The University of Burdwan, INDIA

Received: May 13, 2026

Accepted: October 1, 2026

Published: November 6, 2026

Copyright: © 2026 Abdullah et al. This is an open access article distributed under the terms of the Creative Commons Attribution License, which permits unrestricted use, distribution, and reproduction in any medium, provided the original author and source are credited.

Data availability statement: All data are in the manuscript and/or supporting information files.

Funding: This project is sponsored by Prince Sattam bin Abdulaziz University (PSAU) as part of funding for its PSAU Global South Partnership (GSP) project number

Abstract

The shortage of freshwater and the high energy consumption of traditional desalination methods require the development of renewable energy-based desalination methods such as solar stills. Although solar stills are simple and low cost, their limited productivity remains a barrier to their widespread use. Therefore, the present study aims to enhance the performance of a hemispherical solar still using magnetic rings within the distillation basin. These rings work as fins and a source of a magnetic field that improves evaporation. The novelty of this study lies in the use of a variable-spacing array of magnetic rings by changing the number of rings and analyzing the effect on the performance using comprehensive 4E analysis. The experiments were performed in Al-Madinah Al-Munawarah, Saudi Arabia, during August 2025. The standard solar still (SHSS) was compared with four improved models containing 5, 10, 15, and 20 magnetic rings. The performance of different cases was assessed based on freshwater productivity, energy and exergy efficiencies, economic indicators, and environmental performance. The results indicated a significant enhancement in performance with an increase in the number of magnetic rings. Basin water temperature increased from 45°C in the SHSS to 50.5°C in the MHS-HFM-20. Daily productivity also increased from 4.37 L/m²·day to 7.50 L/m²·day, with an increase of 72%. Thermal and exergy efficiency also improved by 56% and 172%, respectively. Economically, the production cost reduced from $0.011/L to $0.007/L, a reduction of approximately 36% and payback period decreased from 0.27 to 0.176 year with a reduction of 35%. Environmentally, the quantity of mitigated carbon dioxide emissions increased from 2.52 tons to 4.55 tons, reflecting the positive impact of the proposed technology on carbon emission reduction.

PSAU-RDEP-2025-0157 to ASA. The funders had no role in study design, data collection and analysis, decision to publish, or preparation of the manuscript.

Competing interests: The authors have declared that no competing interests exist.

1. Introduction

Energy recession and the deficiency of freshwater represent major problems facing most countries around the world, particularly in desert and remote regions. These two problems continue to increase because of the rapid growth of population, the variation in the global environment, and unsustainable consumption of energy and freshwater [1,2]. Most of the water is salty, which makes it unsuitable for human use, industrial, or agricultural applications. Desalination is an efficient method used to face the problem of freshwater shortage by converting saltwater found worldwide into freshwater [3]. Traditional desalination plants can be sorted into membrane and thermal technologies, such as multi-effect evaporation [4], reverse osmosis [5,6], humidification and dehumidification [4,7], multi-stage flash [8], and hybrid methods [9,10]. Although these technologies efficiently produce the required water in many areas over the world, these methods are high-cost and need high energy consumption to work, leading to a significant pollution problem because these techniques mainly depend on fossil fuels [11,12]. Therefore, it is important to find other methods that relieve renewable energy, especially solar energy. Solar energy is a powerful and friendly alternative to fossil fuels because it is a clean, renewable, and low-cost source of energy [11].

Solar desalination is an efficient method used to tackle the global problem of freshwater lack, especially in regions with higher solar irradiation but limited resources and economy that do not have high energy sources and abilities to construct and operate conventional desalination stations, particularly in North Africa and Middle East countries [13]. The main advantages of solar desalination methods include lower construction and operating costs and absence of environmental pollution [14] Solar still is among solar desalination systems used as the least cost water purification technique, ideal for remote regions. It depends on solar energy as a primary driving energy and requires minimum construction and operation costs and is environmentally friendly. However, its lower daily productivity and poor thermal performance represent the main drawbacks that decrease its widespread [14]. Therefore, various studies have been conducted to improve the performance of solar still performance using new designs or incorporating modification techniques to improve thermal performance and increase the evaporation rate of basin water. Fig 1 shows the various enhancement techniques employed to promote the performance of solar still [15–19].

Hemispherical solar stills (HSSs) are among solar stills that have gained more attention in recent years thanks to their advantages, mainly their ability to efficiently capture solar radiation because of their functional design advantages [13,14]. These stills have hemispherical dome shapes made of transparent glass that achieve absorption of solar radiation in multidirectional cross the day, which increases the collection of solar radiation [20,21]. The inner curvature of domes ensures better areas of condensation, which results in an increase in freshwater production compared to conventional solar stills with flat counterparts, such as single and double solar stills [22,23]. However, HSSs, such as other types of solar still suffer from some restrictions that affect their performance and use, mainly their lower productivity. Additionally, their construction can be more complex and costly, besides the difficulty of their

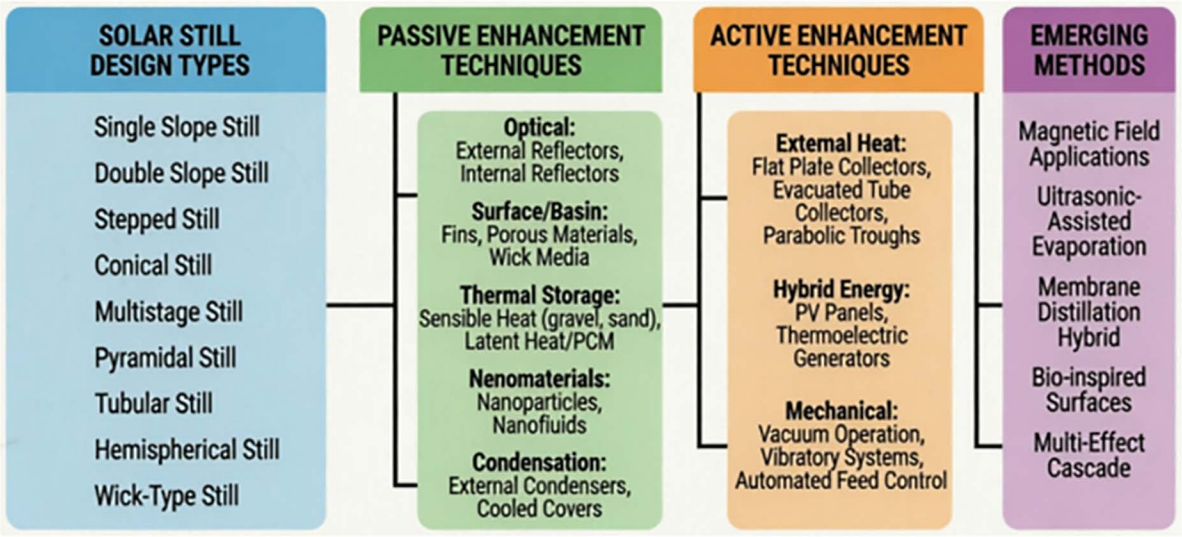

Fig 1. Solar still classification and performance improvement techniques [15–19].

https://doi.org/10.1371/journal.pwat.0000568.g001

maintenance and cleaning because of their curved surface. These limitations can be solved by integrating modification techniques to increase their productivity and enhance performance [24,25]. Table 1 provides some modification techniques that were employed in previous studies to improve the performance and productivity of HSS. The table indicates various modifications. Including storage materials, porous mediums, reflectors, condensers, collectors, …etc. Most studies used a combination of modification techniques, which leads to complexity and cost of the solar still. The improvement in freshwater production ranging from 22.5% to 551.11% and reduced production cost between $0.0148 and $0.00325/L. The use of magnetic sources alone as a proposed modification method in HSS is still limited compared to other techniques, which distinguishes this study.

The use of magnets on the solar still's basin can promote the evaporation process via the effect of the magnetic field. In saline water, water molecules typically adhere to salt ions via weak Van der Waals bonding, leading to a reduction in vapor pressure and an elevation of the boiling point. The magnetic field weakens the Van der Waals force between water molecules and soluble salts, thereby increasing the diffusion coefficient of salt ions and the mobility of water molecules [38]. Therefore, more hydrogen bonds are generated, resulting in larger water clusters compared to non-magnetized water. This clustering facilitates a greater number of water molecules escaping from the water/ vapor interface, thereby improving the evaporation process. Additionally, the decrease in the Van der Waals force by the magnetic field raises vapor pressure, which generates a higher partial pressure difference between the basin water and the glass cover. This, in turn, elevates the evaporative heat transfer coefficient, which leads to an increase in freshwater productivity [39].

The impact of integration of a magnetic field on the evaporation of water has been extensively investigated over the past decade. The evaporation process has been attributed to different mechanisms related to the magnetic field. In early studies by Kitazawa et al. [40] and Nakagawa et al. [41], to investigate the influence of a magnetic field on water evaporation, they illustrated that the magnetic field caused an irregularity in the magnetic susceptibility of vapor at the water-vapor interface, resulting in a magnetic susceptibility gradient that improves a magnetic convection, which increase the evaporation by decreasing the density of the vapor. There also other study investigated the impact on magnetic field on internal energy of the molecules of water [42,43] and on evaporation rate of water [44] The magnetic field was also used to promote the performance of different types of solar stills using different magnetic configurations. Harby et al. [35] used magnetic fins with nano-coated spherical coils in HSS. This resulted in an increase in water yield by

Table 1. A brief review of modifications used in HSS.

Modification	Key results	Ref.
Hanging wick, nanofluids, dish collector, external condenser, and black reflector	The productivity increased from 3.36 to 11.03 L/m2, the energy efficiency increased from 31% to 66.35%, and exergy efficiency increased from 1.8% to 5.92%. The production cost reduced from 0.0148 to 0.0099 $/L, and 3.96 tons of CO_2 emissions were mitigated.	[26]
Film cooling and rotating wick drum	The water productivity and thermal efficiency increased by 64.6%-150.9% and 74.3% - 48.8%, respectively	[27]
Boule's scrubber metallic inox and copper oxide (CuO) nanoparticles	The water yield, thermal efficiency, and exergy efficiency improved by 63.5%, 66.6% and 171.4%, respectively	[28].
Coated recycled cans filled with PCM improved with stainless-steel shavings	The productivity, thermal efficiency, and exergy efficiency increased by 22.5%-123.0%, 22.31–121.03, 48.55%–332.94%, respectively, while production cost, payback times, and CO_2 emissions decreased by 106.0%, 15.6–86.4%, and 24.0–149.2%., respectively,	[29]
Evacuated tube collectors	Productivity and energy efficiency increased by 551.11% and 54.95%, respectively with production costs reduced to $0.00325/L	[30]
Coal powder	The increase in water productivity and thermal efficiency was 41.67% and 41.12%, respectively with a reduction in cost of 63.16%	[31]
Waste aluminum cans filled with copper shavings enhanced-PCM	water yielded enhanced by 108.3%, energy efficiency increased by 112.5%, and exergy efficiency increased by 303.7%	[32].
Wire steel mesh	water yield increased by 61.11%, energy efficiency increased by 60.48%, and exergy efficiency increased by 119.46%	[33]
Copper tubes and natural sponges coated with nanoparticles	water yield increased by 63.46%, production costs improved by 56.41%, the payback period decreased by 33.29%	[34]
Magnetic fins with nano-coated spherical coils	Productivity and thermal efficiency increased by 60.3% and 48.4%, the CPL and payback time reduced to 0.015 $/and 2.81 years, respectively.	[35]
Magnetic field application, nano-enhanced PCM, vertical wick integration	Productivity and energy efficiency increased by 195% and y 65%, with a decrease in the production costs of $0.012/L	[36]
Magnetic fins and recycled cans coated with nanoparticles	Water yield improved by 66.87%, while CPL and payback time decreased by 52.19%.	[37]

https://doi.org/10.1371/journal.pwat.0000568.t001

60.3% and thermal efficiency by 48.4% and decreased the production cost to 0.015 $/and payback time to 2.81 years, respectively, and mitigated about 1.305 kg/yr CO_2 emission. Essa et al. [36] used magnetic field application with vertical wick integration and nano-enhanced PCM in HSS. The results elucidate that productivity improved by 195% and energy efficiency improved by 65%, while production costs decreased to $0.012/L with an enviro-economic parameter of $422.8/year. Attia et al. [37] used magnetic fins with recycled cans coated with nanoparticles in HSS. The use of magnetic fins further increased water yield by 66.87% and reduced CPL and payback time by 52.19%. Alahmadi et al. [45] studied the effect of the number of magnetic poles on the performance of a conical solar distiller. Increasing number to eight poles improved productivity by 08.54%, energy and exergy efficiencies by 107.52 and 238.21% and reduced production cost too 0.0037 $/L with a reduction of 50.13%.

Despite significant progress in the improvement techniques of solar stills' performance in recent years, most of many studies have mainly concerned the use of storage materials, fins, axial cylindrical magnets, or magnetic fields combined with nanoparticles, PCM, wicks, or reflectors. The studies investigating the impact of a magnetic field integrated with the extended surfaces within the solar still remain very limited, especially in HSSs. The novelty of the present work lies in the use of a variable magnetic ring array inside an HSS. Instead of using a single magnetic arrangement or integrating the magnetic field with other additional improvement techniques. This study systematically investigates the effect of both ring number and spatial distribution on the thermal, production, economic, and environmental performance. The proposed modification differs from previous studies using magnetic field through its annular ring geometry, multiple ring

number configurations, variation of controlled spacing, and passive operation without additional active components, and geometry of hemispherical basin. This work aims to consider this research gap by developing an enhanced HSS based on annular fins made of permanent magnets. These magnetic rings simultaneously work as a source of magnetic field and extended heat transfer surfaces that improve the heat transfer and evaporation process in the still. To achieve this objective, experiments were carried out to compare the performance of a traditional solar still with four modified stills containing 5, 10, 15, and 20 magnetic rings. The effectiveness of these modifications was evaluated using comprehensive 4E analysis that integrates new performance indicators in addition to applying of statistical analysis such as ANOVA and t-test. The importance and impact of this study lie in providing a low-cost, simple, and feasible design to enhance the productivity of solar stills, thus improving their potential as a sustainable option for producing freshwater in regions suffering from water shortage and abundant solar radiation.

2. Methodology

2.1 Ethics statement

This study involved laboratory-based experimental evaluation of passive solar distillation systems. No human participants, human data, human biological samples, animals, or field sampling were involved. Therefore, approval from an Institutional Review Board or ethics committee was not required. The study did not pose risks to individual privacy, safety, or welfare. All experiments were performed in accordance with the institutional research regulations of Taibah University, Al-Madinah Al-Munawarah, Saudi Arabia.

2.2 Materials

The ferrite ring magnets were used in this study to generate a permanent magnetic field within the saline water [35,46]. This magnetic field breaks the bonds between water molecules and salt ions, thus decreasing surface tension, which promotes the evaporation rate for the same temperature difference, increasing condensation coefficients, and ultimately freshwater production. At the same time, the ring magnets behave like fins (extended surfaces), so they increase the solid–liquid contact area, which improves convective and evaporative heat transfer at the water–magnet interface, and store sensible heat that is later released to the water as temperature drops. Additionally, ring magnets act as thermal storage mediums that absorb excess heat during the day, thus reducing losses to the surrounding environment, and then release it in the evening or at sunset, which extends the operating hours of the distillation plant and consequently increases productivity. Each annular magnet fin, as shown in Fig 2, was fabricated from Ferrite ring magnet with dark grey color and has an inside diameter of 18 mm, an outside diameter of 30 mm, and a thickness (height) of 5 mm. These rings were selected due to its ability to produce a permanent magnetic field without the need of external electrical input [46]. Furthermore, their ceramic nature provides them with more stability throughout the moderate operating temperature range encountered in the solar still. The thermal properties, given in Table 2, were provided by the manufacturer, while the ring dimensions were determined separately as specifications of the magnets used in the present experiments.

2.3 Experimental setup

Three identical hemispherical stills, as shown in Figs 3 and 4, were designed and fabricated to carry out the experiments. Each HSS was composed of a transparent hemispherical glass cover with a thickness of 3 mm and a diameter of 50 cm, mounted on a stainless-steel basin with a 0.45 m diameter (enclosing an area of 0.159 m^2), 2.5 mm thickness, and 0.1 m depth, as shown in Fig 3(B), as shown schematically in Fig 3. The entire basin was coated with matte black paint to increase the absorption of solar irradiation and insulated from the outer walls with a 5 cm glass-wool layer to decrease heat losses to surrounding. A matte black silicone rubber sealing layer was inserted between the basin and glass cover to prevent any possible vapor leakage. The distilled water from the glass cover flows through a narrow channel located in the inner upper circumference of the basin and is then collected in the bottle, as shown in Fig 4.

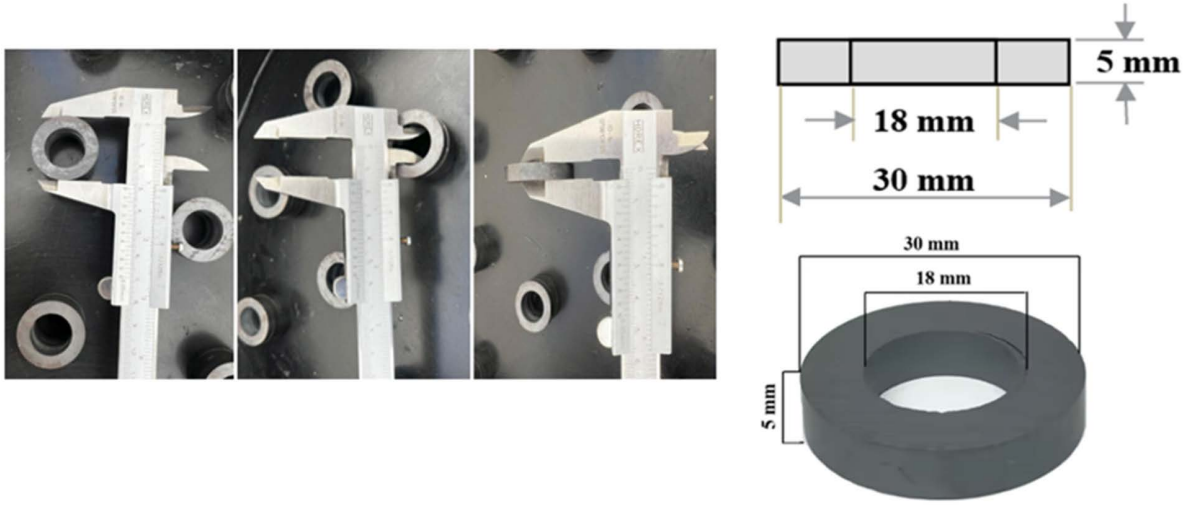

Fig 2. Picture and schematic of the structure of magnetic ring with dimension used in the experiments.

https://doi.org/10.1371/journal.pwat.0000568.g002

Table 2. Thermophysical, geometric, and magnetic specifications of the ferrite ring magnets used in this study [46].

Parameter	Units	Value
Thermal conductivity	$Wm^{-1}K^{-1}$	6.5
Density	kgm^{-3}	490
Specific heat	$Jkg^{-1}K^{-1}$	860
Magnetic field strength	mT	130
Dimensions	mm	30 × 18 × 5

https://doi.org/10.1371/journal.pwat.0000568.t002

2.4 Experimental procedure

A variable array of fins made from identical permanent annular magnets was used throughout the experiments to study the effect of fins on the productivity and performance of solar stills. Each magnet fin was mounted vertically in the water still to simulate extended surfaces and was fully submerged. To achieve maximum magnetic field strength and distribution for the highest solar still productivity, the effect of the number of fins, and hence the spacing between the annular magnet fins, was studied. The number of rings within the water basin was 5 fins (150 mm spacing), 10 fins (120 mm spacing), 15 fins (90 mm spacing), and 20 fins (60 mm spacing). The magnets were arranged in a regular pattern (grid), as presented in Fig 5, to ensure a uniform distribution of the magnetic field and surfaces across the basin, and to prevent clumping that could lead to localized overheating or block light from reaching large areas within the basin.

The experiments were performed in two scenarios, as indicated in Fig 6, over several consecutive days to ensure reproducibility: in the first one, the standard hemispherical still (SHSS), modified hemispherical still with 5 rings (MHS-HFM-5), and modified hemispherical still with 10 rings (MHS-HFM-10) designs were investigated, and in the second scenario, the SHSD, MHS-HFM-15, and MHS-HFM-20 were tested. The basins, between each round, were emptied, cleaned, and then refilled with water of the same depth and salinity. The magnetic rings were repositioned to achieve the same immersion length, maintain all other parameters, such as magnet dimensions, field strength, spacing, and orientation, fixed. For each group of fins, the still was filled with water to the same depth and operated throughout a sunny day. The tests were performed in Al-Madinah, a Saudi Arabian city. Each experimental run was carried out across a complete

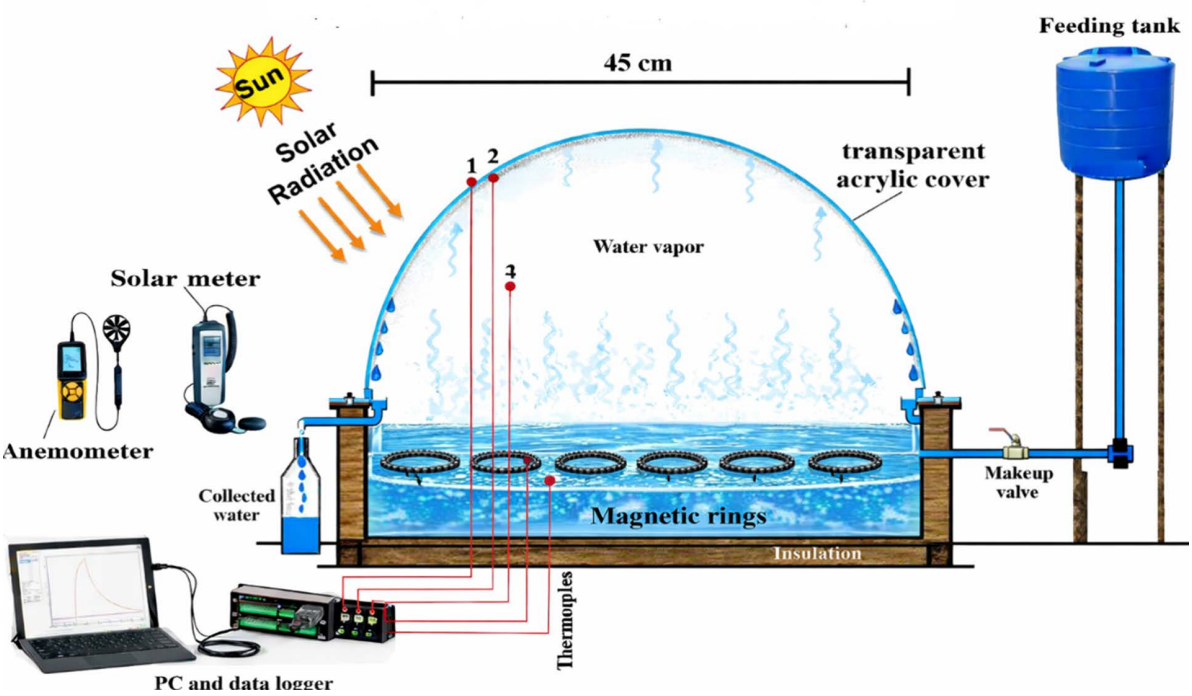

Fig 3. Schematic of the HSS experimental setup with main components and locations of the measuring instruments.

https://doi.org/10.1371/journal.pwat.0000568.g003



Fig 4. Photograph of the HSS experimental setup with three identical hemispherical stills.

https://doi.org/10.1371/journal.pwat.0000568.g004

daily operating period from 07:00–21:00, corresponding to 14 h, which covers the entire daytime heating, maximum evaporation, and post-solar productivity periods. The experiments were carried out during various consecutive days of August 2025 under almost identical ambient conditions. The experiments were repeated to verify the measurements' reproducibility, and the results used to evaluate the performance of different designs represent the average values of repeated measurements.



Fig 5. Arrangement of ferrite magnetic rings inside the still basin for the modified configurations, corresponding to ring spacings of 150, 120, 90, and 60 mm, respectively.

https://doi.org/10.1371/journal.pwat.0000568.g005

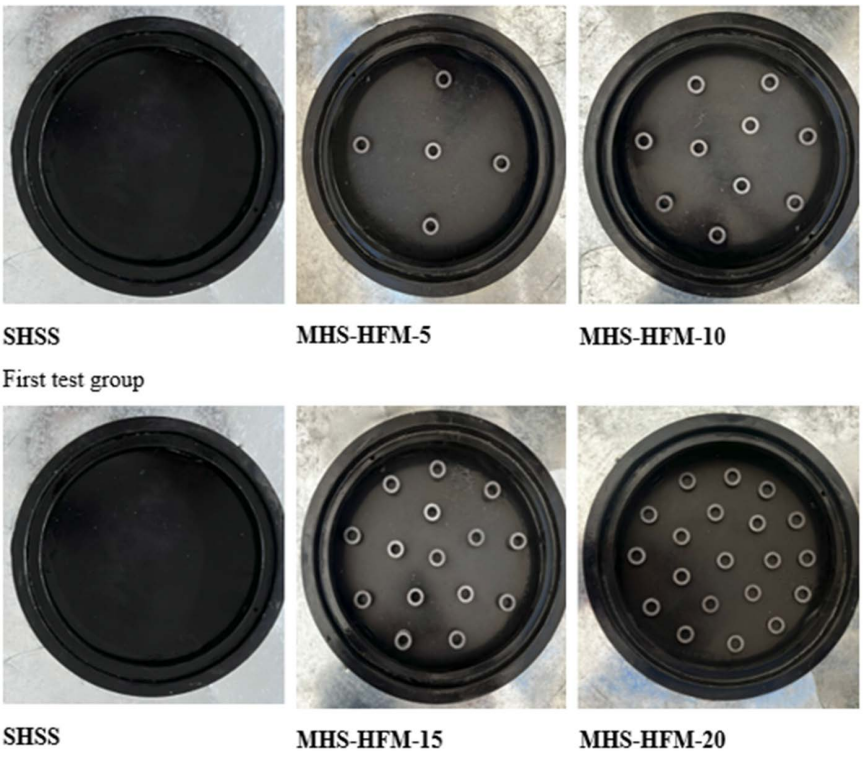

Fig 6. Experimental configurations investigated in the two test groups: SHSS, MHS-HFM-5, and MHS-HFM-10 in the first group, SHSS, MHS-HFM-15, and MHS-HFM-20 in the second group.

https://doi.org/10.1371/journal.pwat.0000568.g006

The saline water used in the distillation basins came from the city of Yanbu with a salinity (TDS) of 40,000 ppm and a pH level of 7.5. The distilled water produced in the experiment had a pH of 7.3 and a salinity of 88 ppm. This met WHO safe drinking water criteria (<600 ppm TDS and 6.5 – 8.5 pH).

2.5 Measurements and uncertainty

In order to estimate the performance of HSS under different number of rings, various measuring instruments were used to measure and record the different variables during the experiments, including ambient conditions (solar radiations, ambient air temperature, relative humidity, and wind speed) temperature of basin water, temperature of inner and outer glass, and freshwater yield throughout the day. The measuring instruments with their ranges, accuracies, and uncertainties are listed in Table 3. The temperature sensors used to measure the ambient temperature and the temperatures of different components of solar still, including water basin and inner and outer glass cover. Temperature and solar radiation sensors were connected to an Arduino data acquisition system connected to a computer to enable real-time monitoring and recording. While wind speed was measured using a digital anemometer. Multiple experimental runs were carried out on the proposed HSS cases to ensure consistency and repeatability of the data under identical ambient and operational conditions. The uncertainties of measuring instruments were estimated using Holman equation [47] as follows:

$$U = \sqrt{\left(\frac{\partial J}{\partial X_1}\right)^2 g_1 + \left(\frac{\partial J}{\partial X_2}\right)^2 g_2 + \left(\frac{\partial J}{\partial X_3}\right)^2 g_3 .. \left(\frac{\partial J}{\partial X_n}\right)^2 g_n} \quad (1)$$

Where *U is* the uncertainty during the experiments, *n* is the number of variables, *g* is the uncertainty of the measured value. The mean uncertainty for temperature measurement was ± 0.2%, distilled water yield was ± 0.87%, the daily energy efficiency was ± 1.08% and the exergy efficiency was 1.1%.

3. 4E analysis of solar still performance

The 4E analysis, including Energy, Exergy, Economics, and environmental analyses, is a comprehensive and integrated approach for assessing the performance and efficiency of solar stills systems, where each indicator provides precise insight into the sustainable dynamics of solar stills. Energy efficiency was determined based on the first law of thermodynamics; it indicates the amount of absorbed solar energy used in the evaporation of basin water. The latent heat of vaporization (h_{fg}) was determined as a function of basin water temperature using a standard correlation commonly used in solar still analysis. Exergy analysis aims to identify the sources of usable energy loss, such as losses in the basin and glass cover, and helps to decrease the heat loss and improve the quality of energy. The exergy input (Ee_i) was determined using the Petela radiation exergy model, while useful output exergy (Ee_o) was evaluated from the latent heat associated with freshwater evaporation. In the economic analysis, initial, operating, maintenance, and other costs are estimated against freshwater production, using different indicators such as the cost per liter (CPL) and the payback period. Environmental analysis elucidates the environmental benefits of the solar still by estimating the carbon emissions saved

Table 3. Measuring instruments, measurement ranges, accuracies, and associated uncertainties.

Parameter	Instrument	Range	Accuracy	Uncertainty
Solar radiation (W/m^2)	Solar power meter (SPM 1116SD)	0.0 to 2000 W/m^2	±1 W/m^2	0.12%
Temperature (^{o}C)	Temperature sensor (DS18B20)	0-120 ◦C	±0.2 ◦C	0.32%
Wind speed (m/s)	Anemometer (LM-8102)	0.4–30 m/s	±0.1 m/s	1.45%
Water yield (kg)	Load cell 190	0–20 kg	±5 g	0.18%

https://doi.org/10.1371/journal.pwat.0000568.t003

compared to traditional desalination methods and identifying the environmental effects of the materials used in manufacturing. The environmental analysis accounts for the embodied energy needed to fabricate the solar still and the radiational energy related CO_2 emissions produced by solar driven freshwater production across the lifetime of the still. Table 4 provides the important equations used to determine each indicator for the different 4E analyses.

The embodied energy (E_{Embo}) presented in Equation 15 was calculated by considering the main materials used in the manufacture process of different components of solar still, such as glass cover, galvanized iron, paint, insulation, and other things. Table 5 indicates the total embodied energy for different configurations of HSS.

3.1 Heat transfer analysis

The heat transfer in an HSS was studied to determine the heat transfer mechanism between basin water and the glass cover, which controls both evaporation and condensation processes. The heat transfer between water in the basin and the glass cover is expressed as follows [37].

$$q_{total_{w,g}} = q_{con_{w-g}} + q_{rad_{w-g}} + q_{ev_{w-g}} \tag{17}$$

Table 4. Equations, definitions, and reference basis used for the 4E assessment of the investigated HSS [45,48,49].

1. Energy analysis:		
$\eta_{en} = \frac{\dot{E}_{out}}{\dot{E}_{in}} = \frac{\sum m_{fw} \times h_{fg}}{\sum A_b \times \Delta I_t \times \Delta t}$ Where: m_{fw} is the produced freshwater yield (kg/hr), I_t is the sun intensity, Δt is time interval (hr), A_b is the basin area, and h_{fg} is the latent heat calculated as follows $h_{fg} = 2.4935 \times 10^6 \times [1 - T_{bw}(9.4779 \times 10^{-4} + 1.3132 \times 10^{-7} \times T_{bw} - 4.794 \times 10^{-9} \times T_{bw}^2$		(2) (3)
2. Exergy analysis		
$\eta_{ex} = \frac{\sum \dot{Ee}_o}{\sum \dot{Ee}_i}$ Where $\dot{Ee}_i$ and $\dot{Ee}_o$ are the input exergy and output exergy, respectively, given as follows $\dot{Ee}_i = A_b \times \Delta I_t \left[1 - \frac{4}{3}\left(\frac{T_a+273}{T_{sun}}\right) + \frac{1}{3}\left(\frac{T_a+273}{T_{sun}}\right)^4\right]$ $\dot{Ee}_o = m_{fw} \times h_{fg} \left(1 - \frac{T_a}{T_w+273}\right)$		(4) (5) (6)
3. Economic analysis		
Cost per liter ($/l)	$CPL = \frac{TAC}{MA}$	(7)
Total annual cost ($)	$TAC = CFY + AMC - ASC$	(8)
Annual yield	$MA = m_d * Nday$	(9)
Payback period	$Pp = \frac{\ln(\frac{CF}{CF-P*i})}{\ln(1+i)}$	(10)
Annual cash flow	CF = MA*Mv, Mv is market/sealing value	(11)
Levelized Cost of Water (LCOW),	$LCOW = \frac{P \times CRF + O\&MC}{MA}$ Where O&MC is operating and maintenance costs = 15%P	(12)
Benefit-Cost Ratio (BCR)	$BCR = \frac{CF \times \left(\frac{(1+i)^n-1}{i(1+i)^n}\right)}{P+O\&MC}$	(13)
Net Present Value (NPV)	$NPV = \sum_{t=1}^{n} \frac{(CF-O\&MC)}{(1+i)^t} - P$	(14)
4. Environmental analysis		
The net of CO_2 mitigation(ton)	$NM_{CO2} = \frac{\mu_{CO_2} \times ((E_{n,out,ann} \times n) - E_{Embo})}{1000}$ Where μ_{CO_2} is the CO_2intensity=1.58 kg_{CO2}/KWH [50]	(15)
The carbon credit ($) [50]	$CC_{CO2} = NM_{CO2} \times \$_{CO2}$ where $\$_{CO2}$ is s the cost of CO_2 traded per ton = 14.5$/ton	(16)

https://doi.org/10.1371/journal.pwat.0000568.t004

Table 5. Embodied energy of the components used in different cases of HSS.

Component	Energy density (kWh/kg)	Component mass (kg)	SHSS	MHS-HFM-5	MHS-HFM-10	MHS-HFM-15	MHS-HFM-20
Galvanized iron: basin and frame	13.90	8.00	111.200	111.200	111.200	111.200	111.200
Glass	4.16	5.00	20.800	20.800	20.800	20.800	20.800
Insulation	5.56	0.50	2.780	2.780	2.780	2.780	2.780
Black paint	25.00	0.40	10.000	10.000	10.000	10.000	10.000
Rubber gasket	3.28	0.20	0.656	0.656	0.656	0.656	0.656
Feeding tank	21.40	3.00	64.200	64.200	64.200	64.200	64.200
Brass valves	17.22	0.21	3.616	3.616	3.616	3.616	3.616
Ferrite magnetic rings	**0.30***	0/ 0.025/ 0.050/ 0.075/ 0.100	0	0.0075	0.0150	0.0225	0.0300
Total embodied energy, (kWh)			**213.2522**	**213.2597**	**213.2672**	**213.2747**	**213.2822**

https://doi.org/10.1371/journal.pwat.0000568.t005

where $q_{con_{w-g}}$, $q_{rad_{w-g}}$, and $q_{ev_{w-g}}$ are the portions of heat transferred by convection and radiation, and evaporation respectively, calculating as follows:

$$q_{con_{w-g}} = h_{con_{w-g}} \left(T_w - T_{gi}\right) \tag{18}$$

where $h_{con_{w-g}}$ is convective heat transfer coefficient, calculating corresponding to the partial saturated vapor pressure of water (P_w) and that of cover temperature (P_g) using by Dunkle [45]

$$h_{con_{w-g}} = 0.884 \left[\left(T_w - T_{gi}\right) + \frac{(P_w - P_g)(T_w + 273)}{268900 - P_w}\right]^{\frac{1}{3}} \tag{19}$$

$$P_w = exp\left[25.317 - \frac{5144}{T_w + 273.15}\right] \tag{20}$$

$$P_g = exp\left[25.317 - \frac{5144}{T_{gi} + 273.15}\right] \tag{21}$$

The radiation heat transfer is calculated as the follows [46]:

$$q_{rad_{w-g}} = h_{rad_{w-g}} \left(T_w - T_{gi}\right) \tag{22}$$

$$h_{rad_{w-g}} = \varepsilon_{eff}\, \sigma \left[(T_w + 273.15)^2 + (T_{gi} + 273.15)^2\right] \times (T_w + T_{gi} + 546.3) \tag{23}$$

Where σ is Stefan–Boltzmann constant ($5.67*10^{-8}$ W/m^2.K^4), and the ε_{eff} is the effective emissivity for each water emissivity (ε_w) and glass emissivity (ε_g) given as follows [47]:

$$\frac{1}{\varepsilon_{eff}} = \left(\frac{1}{\varepsilon_w} + \frac{1}{\varepsilon_g} - 1\right) \tag{24}$$

The evaporative heat transfer was calculated using the following equations [48]

$$q_{evw-g} = h_{ew-g}\left(T_w - T_{gi}\right) \tag{25}$$

$$h_{evw-g} = 16.27 \times 10^{-3}\, h_{condw-g}\, \frac{(P_w - P_{gi})}{(T_w - T_{gi})} \tag{26}$$

The total internal heat transfer coefficient between basin water and the inner glass cover was determined as follows [49]:

$$h_{totalw-g} = h_{condw-g} + h_{evw-g} + h_{radw-g} \tag{27}$$

The external convective heat loss from the glass cover to the ambient air was evaluated as

$$q_{conv,g-a} = h_{conveg-a}\left(T_{go} - T_a\right) \tag{22}$$

4. Results and discussion

4.1 Performance analysis of solar still

The hourly variation of average ambient parameters is shown in Fig 7, indicating the daily trends in solar irradiance, ambient air temperature, humidity, and wind speed, which are key variables affecting the productivity of solar stills. Solar irradiance gradually increased from lower values below 200 W/m² in the morning, then rapidly peaked at around 1000 W/m² around midday, before gradually decreasing until the evening. This increase in irradiance results in an increase in basin water temperature and hence a higher evaporation rate, directly affecting the freshwater production during the afternoon hours. The ambient air temperature exhibited similar trend, starting with lower values of 29.7 °C in the morning, reaching its maximum value around 45.2°C during the afternoon and then decreased again at night. The rise in ambient temperature

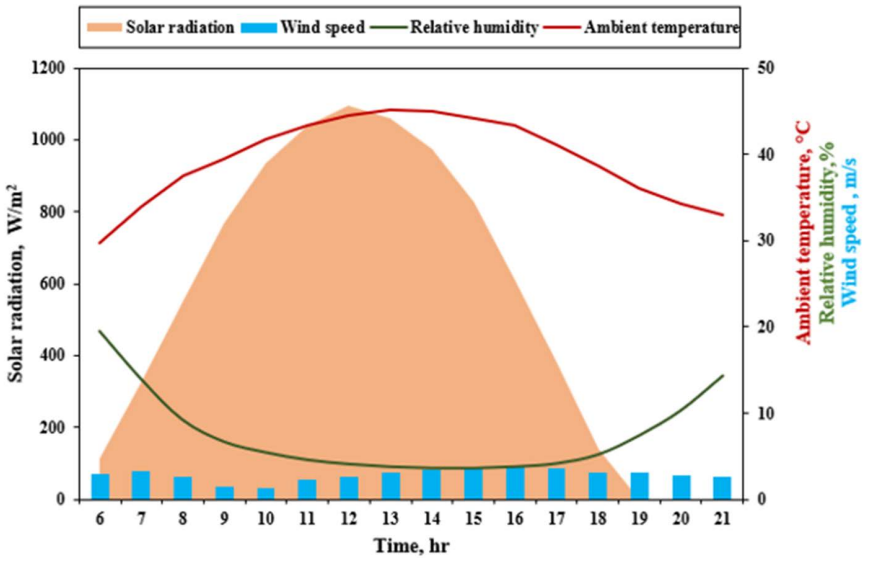

Fig 7. The daily variation of ambient conditions.

https://doi.org/10.1371/journal.pwat.0000568.g007

decreases heat loss and increases the vapor pressure difference between the water surface and the glass cover, resulting in promoting evaporation and condensation processes. Conversely, the relative humidity had the opposite trend, starting higher in the morning and then gradually decreasing until noon before rising again toward evening. Lower relative humidity is a significant variable in increasing the evaporation rate because dry air has a higher capacity to absorb water vapor, thus enhancing the productivity of the still during low humidity periods. Wind speed is estimated to be between 1.8 and 3.5 m/s across the day. Moderate wind speeds can improve heat transfer from the still cover to the surrounding environment, decreasing the temperature of the condensation surface and hence increasing the vapor condensation rate. Therefore, the increase in solar radiation and ambient temperature along with low humidity during midday hours represents the optimal conditions for the highest productivity of freshwater during the day.

The evolution of water and inner glass temperatures and temperature differences during the different operating hours of all cases are indicated in Fig 8. The basin temperature plot highlights that all configurations exhibited a symmetrical bell curve, peaking at 13–14 P.M. The SHSS achieved the lowest value of 60°C at the at 13 P.M, while MHS-HFM-20 had

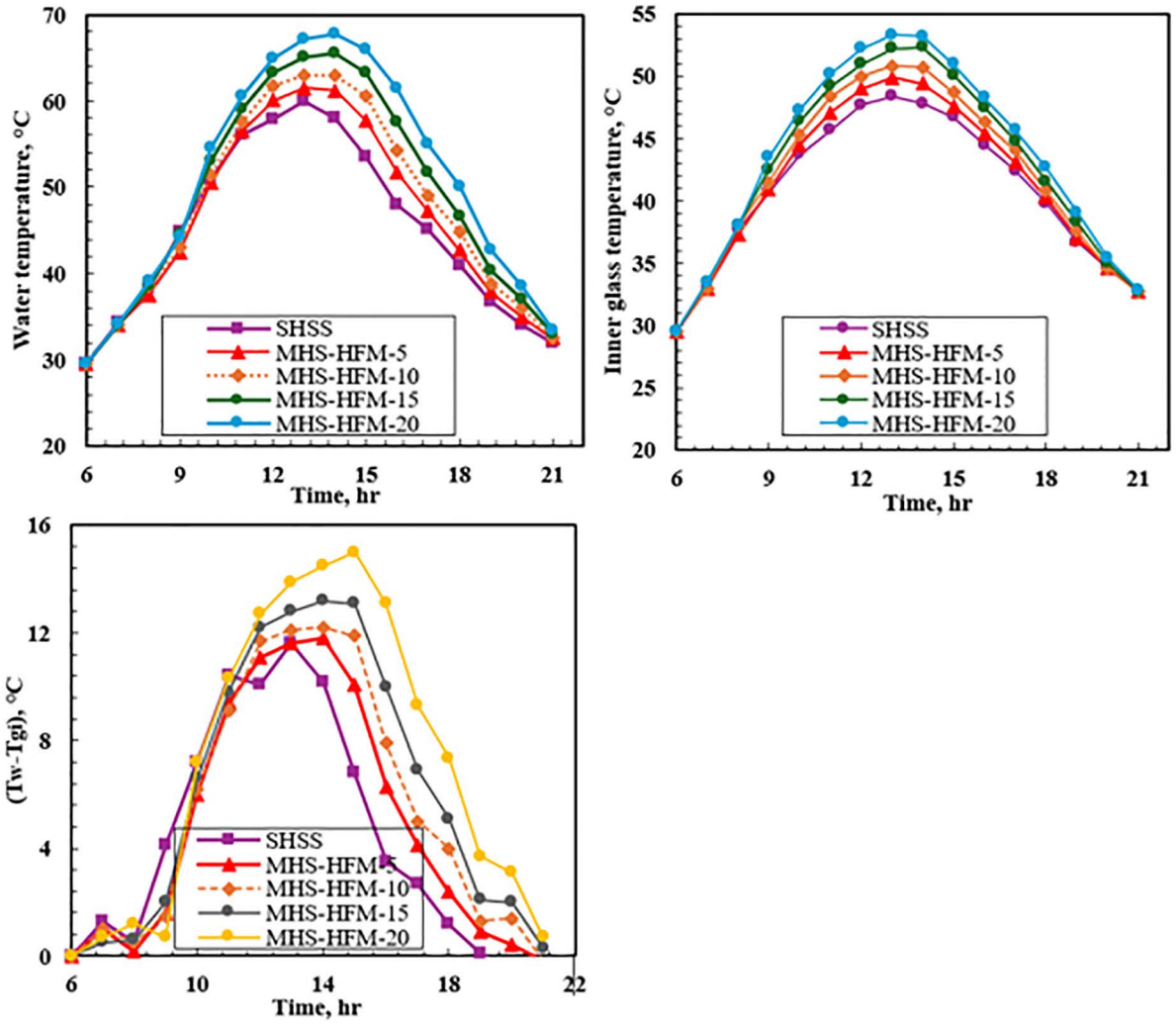

Fig 8. Hourly variations in basin water temperature, inner glass cover temperature, and the temperature difference (Δ T = Tw-Tgi) for SHSS and modified configurations during the daily operating period.

https://doi.org/10.1371/journal.pwat.0000568.g008

the highest temperature of approximately 67.7°C, representing a difference of 7.2°C. This gradual increase in basin water temperature with the rise in the number of magnetic fins is due to several fundamentally generated magnetic fields that influence water molecules and decrease the water's surface tension and increase molecular mobility, which improves the evaporation rate. Additionally, the fins act as thermal fins, increasing the heat transfer surface area between the water and the basin, thereby enhancing the absorption and distribution of solar energy and providing additional paths for heat transfer from the basin to the water. The lower spacing between the fins as the number of rings increases produces an overlap in magnetic fields, which creates improved convection currents within the water. This also minimizes the formation of stagnant zones and achieves uniform heat distribution. The inner glass temperature plot elucidates that the values exhibited the same trend but at lower temperatures. The MHS-HFM-20 achieved the maximum temperature of 53.3°C, compared to 48.4°C for the SHSS, with a difference of 4.9°C. This rise in temperature reveals a rise in the amount of water vapor rising from the basin. This vapor carries latent heat energy that condenses on the inner surface of the glass, which increases its temperature. The magnetic fins also improve the movement of convection currents within the cover, which decreases the heat loss and keeps higher glass temperatures. Meanwhile, the inner glass temperature remains lower than the water temperature, which keeps favorable conditions for condensation. The third plot indicates the temperature difference between the basin water and the inner glass (Tw-Tgi), which is an essential parameter in the evaporation rate according to Dunkel's equation. The figure clearly confirms the superiority of modified stills, as the MHS-HFM-20 had the highest temperature difference of approximately 15°Ccompared to 10°C of SHSS, representing nn increase of 50% in the driving force for evaporation. The increase in temperature difference with an increase in magnetic rings emphasize that higher fin density improves heat transfer and generates greater temperature gradients. This is attributed to the increase in the number of fins decrease the spacing between them from 150 mm to 60 mm, resulting in: (1) an increase in the overall magnetic field strength within the basin that improves the impact on the physical properties of water; (2) a more uniform distribution of magnetic fields, minimizes the creation of weak field regions; and (3) a rise in the effective thermal surface area for heat transfer, as each fin acts as an additional source of heat absorption and transfer. These findings illustrate the significant improvement in freshwater productivity observed in the modified stills, as the evaporation rate is directly proportional to the temperature difference between the water and the glass, a variable greatly improved by the magnetic modification.

The experimental result of average basin water temperature, as presented in Fig 9 highlights an obvious upward trend with the increasing number of magnet rings, compared to SHSS. The water temperature recorded the lowest temperature of 45°C for SHSS, increased to 46°C for MHS-HFM-5 with an improvement of 3.50%, then to 47.28°C for MHS-HFM-10 with an increase of 6.3%, and 48.86°C for MHS-HFM-15 with an enhancement of 10.27%, reaching a maximum value of 50.5°C for MHS-HFM-20 with an increase of 15.1%. This gradual improvement in basin water temperature is a result of two synergistic impacts: First, the magnetic field emitted by the magnetic rings produces a force that decreases the fragile van der Waals bonds between water molecules and salt ions. This raises the ion diffusion coefficient and enhances the mobility of water molecules, consequently increasing the partial vapor pressure and improving the pressure differential driving evaporation. This, in turn, promotes the evaporative heat transfer coefficient and increases the basin water temperature. Second, the magnetic rings operate as thermal fins that increase the contact area, which enhances convection and evaporative heat transfer at the water-magnet interface. They also act as a sensible heat storage medium, absorbing additional heat during peak solar irradiation hours and gradually releasing it as the temperature drops. This extends the effective evaporation period and maintains high thermal levels in the basin. These findings agree with the scientific principles elucidating that the use of a magnetic field on saline water decreases surface tension and slightly reduces specific heat capacity, which allows for higher evaporation rates under the same temperature difference. The uniform distribution of the rings in a basin ensures homogeneity in magnetic field intensity and minimizes localized heat concentration, thus improving thermal absorption efficiency and efficiently converting solar energy into evaporative energy.

Fig 10 shows total freshwater productivity with percentage improvement for different cases. The figure indicates a clear gradual increase in freshwater yield with an increase in the number of magnetic rings, or decrease in the distance

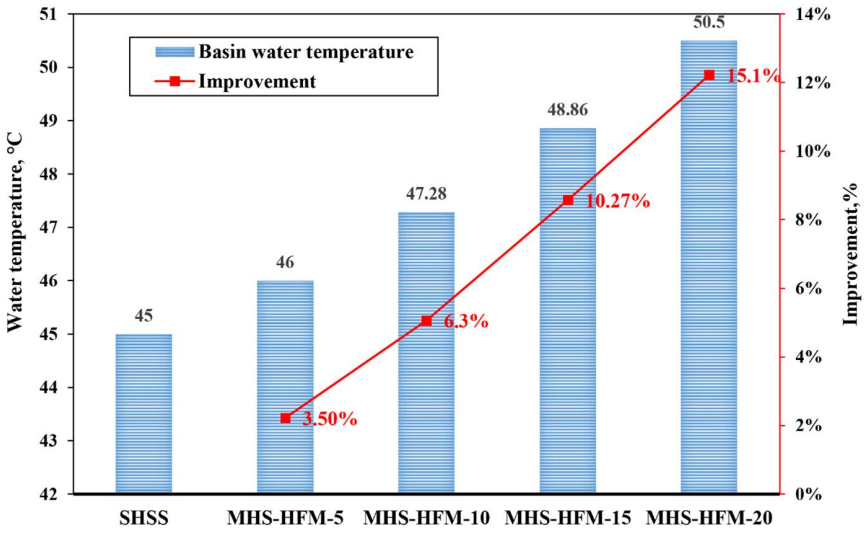

Fig 9. The average temperature of basin water for different cases.

https://doi.org/10.1371/journal.pwat.0000568.g009

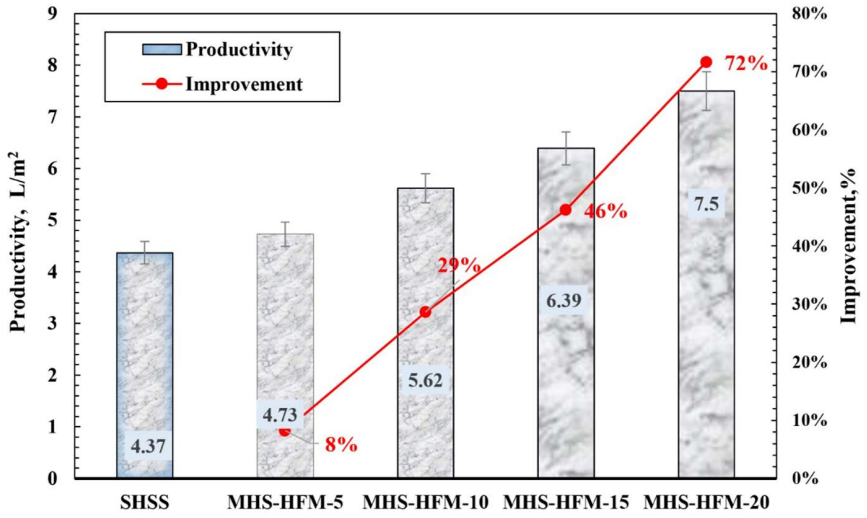

Fig 10. Daily freshwater productivity and percentage improvement relative to SHSS for the standard and modified stills containing 5, 10, 15, and 20 magnetic rings.

https://doi.org/10.1371/journal.pwat.0000568.g010

between rings, inside the basin. In the SHSS, productivity was the lowest with a value of 4.37 L/m²·day, increased to 4.73 L/m²·day in the MHS-HFM-5, with an increase of nearly 8%. With the rise in the number of rings to ten in the MHS-HFM-10, the productivity increased to 5.62 L/m²·day, representing a 29% improvement. This upward trend continued in the MHS-HFM-15, achieving productivity of 6.39 L/m²·day, with a 46% improvement. The highest increase in productivity of 7.50 L/m²·day was achieved by the MHS-HFM-20, with a significant improvement of 72% compared to the SHSS. This direct enhancement in productivity is linked to the rise in basin water temperature owing to the magnetic field impacts of the rings. The magnetic rings act as extended surfaces, increasing the heat transfer area between the water and the basin

surface, which promotes the convection and evaporation heat transfer coefficients. The magnetic field also influences the molecular structure of the saline water, which increases molecular motion and hence the vapor pressure at the water surface. Consequently, the evaporation rate increases based on the fundamental mass transfer relationship that links the evaporation rate to the vapor pressure differential and water temperature. The increase in basin water temperature, in addition to the higher vapor pressure differential, improves evaporation and condensation. The gradual increase in freshwater yield should be illustrated together with the thermal response of the solar still instead of as an isolated output variable. Furthermore, the increase in the number of magnetic rings simultaneously reduced their spacing from 150 to 60 mm, which increases the effective heat transfer area within the basin. Therefore, the average temperature of water increased from 45 °C in the SHSS to 50.5 °C in MHS-HFM-20, along with an increase in the maximum temperature difference from approximately 10–15 °C. This larger temperature difference leads to a stronger thermal driving force for evaporation and condensation, which illustrates the improvement in daily productivity from 4.37 to 7.50 L m^{-2} day^{-1}, with an enhancement of 72%.

The effect of magnetic ring numbers on energy efficiency is shown in Fig 11 along with the percentage improvement. Energy efficiency is a direct indicator of the efficiency of converting solar energy into potential energy for evaporation of saline water in the basin. The SHSS exhibited the lowest energy efficiency of 27%, while it increased to 29% in the

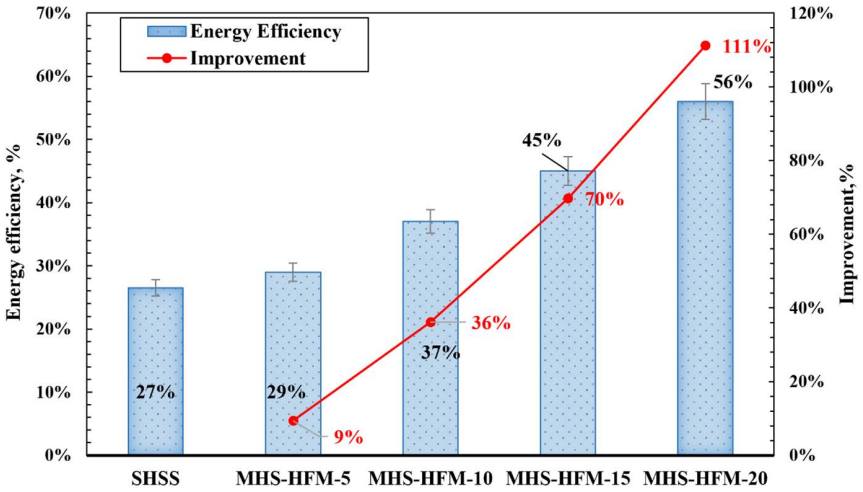

Fig 11. Energy efficiency and corresponding enhancement relative to SHSS for the different magnetic ring configurations. Fig 12 shows the exergy efficiency along with the percentage improvement for modified solar stills compared to SHSS. The figure shows an increasing trend with the use of rings which reflects the gradual enhancement in energy utilization within the system thanks to the use of magnetic rings. Exergy efficiency differs from energy efficiency as it indicates how the still efficiently converts available solar energy into useful work corresponding to evaporation and distilled water production, considering the irreversibility of thermal processes and heat losses. The results illustrate that the exergy efficiency increased from 1.31% in the SHSS to 1.64% in the MHS-HFM-5, with an improvement of 25% rose to 2.10%, with an increase of 60% in the MHS-HFM-10. The upward trend continued in the MHS-HFM-15 achieving an exergy efficiency of 2.70%, an improvement of 106%. The MHS-HFM-20 case exhibited the highest exergy efficiency of 3.56%, an increase of 172%. This increase in exergy efficiency is attributed to the ability of the magnetic rings to improve thermal properties and energy transfer within the basin. They increase the heat exchange area and help distribute heat more evenly inside the basin that decreases the heat loss. The magnetic rings work as a thermal storage medium that reduces the local temperature gradients, thus decreasing the entropy generated at the basin-water interface. On the other hand, the low exergy efficiency achieved in this study is expected in passive solar stills, as the incident solar radiation has relatively high exergy, whereas the useful output is obtained across low-temperature evaporation and condensation. Therefore, only a small portion of the available solar exergy is converted into useful exergy corresponding to freshwater production, while the remainder is destroyed via irreversible heat transfer processes and rejected to the surroundings. Furthermore, the main sources of exergy destruction are the large temperature differences included in heat transfer from the basin to water, solar absorption, evaporation at the water surface, condensation at the glass cover, and heat rejection from the glass to the ambient environment. The increase in the number of magnetic ring fins improves useful evaporation and decreases the relative exergy destruction in the basin, illustrating the progressive enhancement in exergy efficiency with increasing ring density.

https://doi.org/10.1371/journal.pwat.0000568.g011

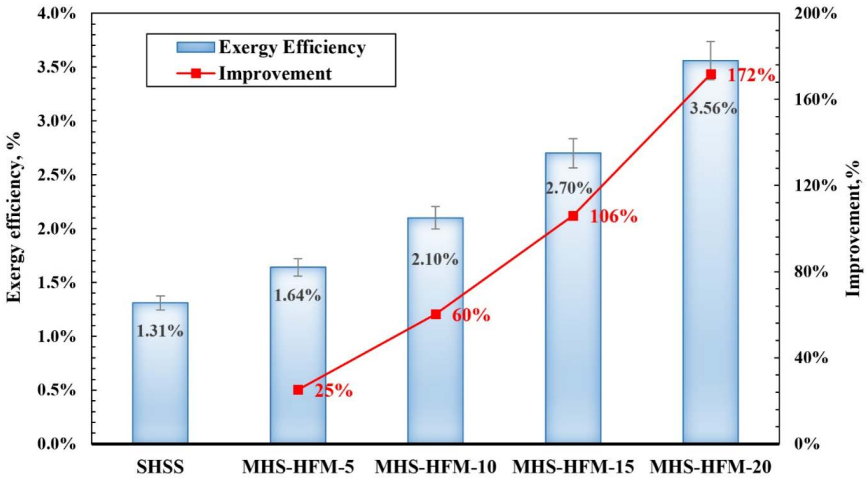

Fig 12. Exergy efficiency and corresponding improvement relative to SHSS for the investigated configurations.

https://doi.org/10.1371/journal.pwat.0000568.g012

MHS-HFM-5 with an increase of 9%. The efficiency increased with the rise in the number of rings to 37%, a 36% increase in the MHS-HFM-10 and to 45%, a 70% improvement in the MHS-HFM-15. The MHS-HFM-20 achieved energy efficiency of 56%, representing an increase of 111%. This increase is a direct result of using the magnetic rings, which increased basin water temperature and hence evaporation rate which translated to an increase in productivity besides the improvement in the thermal performance of the solar still. The increases in evaporation rate reflect the improvements in the efficient use of absorbed solar energy, which results in the conversion of a larger portion of solar radiation into latent heat of evaporation. This is demonstrated by the continuous enhancement in energy efficiency with the increasing number of magnetic rings.

Table 6 provides the results of the exergy destruction distribution within the solar still. The results reveal dynamic behavior reflecting the redistribution of thermodynamic losses inside the still with the increase in the magnetic ring density. The calculation of exergy destruction distribution starts with determining the input and output exergy using equations 5 and 6, as the difference between these two parameters represents the total exergy destruction. The exergy balance was applied to calculate the exergy destruction of each component of still, mainly basin, water, and glass. The exergy destruction of each component was divided by total exergy destruction to determine its percentages. Basin destruction gradually reduced from 78.4% in the SHSS to 76.2% in MHS-HFM-5, then to 74.5% in MHS-HFM-10, 72.3% in MHS-HFM-15, and finally to 70.1% in MHS-HFM-20, which represents an overall reduction of 10.6%. This reduction is due to enhanced heat transfer from the basin to the water because of the dual effect of the magnetic rings, which act as fins and storage material that promotes heat transfer and decreases entropy generation at the basin-water interface. In contrast, water mass destruction rose from 14.2% in SHSS to 18.8% in MHS-HFM-20, representing a total increase of 32.4%. This increase

Table 6. Distribution of exergy destruction and overall exergy efficiency for SHSS and the modified configurations containing 5–20 magnetic rings.

Exergy Component	SHSD	MHS-HFM-5	MHS-HFM-10	MHS-HFM-15	MHS-HFM-20
Basin Destruction	78.4%	76.2%	74.5%	72.3%	70.1%
Water Mass Destruction	14.2%	15.5%	16.2%	17.5%	18.8%
Glass Cover Destruction	6.2%	6.8%	7.3%	7.8%	8.0%
Exergy Efficiency	**1.21%**	**1.45%**	**1.94%**	**2.38%**	**3.12%**

https://doi.org/10.1371/journal.pwat.0000568.t006

reveals the intensification of evaporative activity within the water mass rather than indicating a negative trend. The magnetic field decreases the surface tension and increases the ion diffusion coefficient, thus increasing the entropy generation rate associated with mass and liquid-vapor phase transfer processes. Glass cover destruction also exhibited a slight increase from 6.2% in SHSS to 6.8%, 7.3%, 7.8%, and 8.0% in the modified stills, respectively. This is due to improved condensate vapor rate and a higher temperature difference between the water and the glass cover, improving heat transfer by convection and condensation but also produces higher entropy at the glass interface. These shifts in the destruction distribution culminate in a clear improvement in the overall exergy efficiency from 1.21% to 3.12% in MHS-HFM-20 cases with a 157.8% improvement. These results demonstrate that the magnetic field not only decreases losses in the basin but also enhances the quality of solar energy conversion into useful work (evaporation) by improving the dynamic balance between the system components and decreasing the overall thermal resistance. This agrees with the second law of thermodynamics, which indicates that decreasing damage in the main components (the basin) along with increasing useful activity in the secondary components (the saline water) results in increasing overall exergy efficiency.

Fig 13 shows the energy distribution and heat loss for the different systems. The evaporation energy (useful) increased from 311 W/m² in the SHSS to 475 W/m² in the case of MHS-HFM-20. This direct gain is a consequence of the impact of the magnetic field in decreasing surface tension and increasing the basin water temperature (from an average of 45°C to 50.5°C), which accelerates the phase transition. On the other hand, the higher operating temperatures increase the heat loss components. The internal heat transfer from the basin water to the glass cover represents convection loss (Conv w→g), rose from approximately 75–100 W/m², because of the increased density difference between the hot water surface and the cooler glass cover, which promotes natural convection currents. Convection radiance loss (Rad w→g) also rose from 95 to 135 W/m² according to the Stefan-Boltzmann law, which relates radiant energy to absolute temperature. As for the external loss from the cover to the surrounding, the convection loss (Conv g→a) significantly increased from 15 to 70 W/m² thanks to the increased temperature of the external glass cover and its interaction with the wind and surrounded air. The radiative loss towards the sky (Rad g→sky) rose from 75 to 110 W/m² due to the emission of more intense infrared waves from the hot glass, while the bottom loss (Bottom) increased slightly from 15 to 25 W/m² due to increased thermal conductivity through the insulation. The total loss elucidates that the total overall heat loss from the system

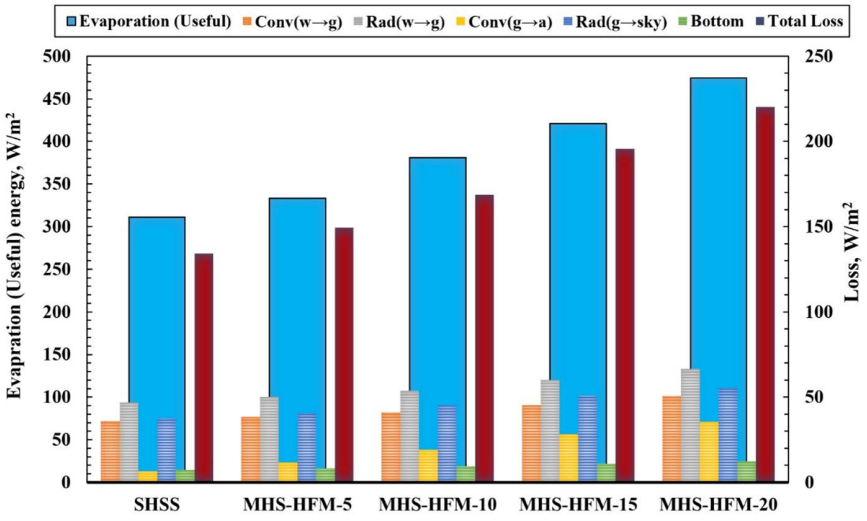

Fig 13. Useful evaporative energy, internal heat transfer components, and external thermal losses for SHSS and the modified magnetic ring configurations.

https://doi.org/10.1371/journal.pwat.0000568.g013

increased from 140 W/m² in the SHSS to 220 W/m² in the enhanced case. However, the increase in useful energy of 164 W/m² far outweighs the increase in total loss (80 W/m². This scientifically emphasizes that the magnetic field increased the water temperature in the basin and directed the resulting additional heat towards the evaporation process with higher conversion efficiency. This resulted in a net enhancement in thermal performance despite the high loss rates associated with high temperatures.

4.2 Economic analysis results

Fig 14 presents the cost per liter (CPL) with the percentage reduction for different designs, clearly indicating the downward trend in the production cost with the increase in the number of magnetic rings within the basin. The CPL represents the actual cost of producing one liter of freshwater across the operational lifetime of the still compared to the capital and operating costs. The CPL of the SHSS was $0.011, and it decreased to $0.0105, $0.009, $0.008 in the MHS-HFM-5, MHS-HFM-10, and MHS-HFM-15, representing a reduction of approximately 5%, 18%,27%, respectively. The lowest value was recorded in the MHS-HFM-20 case at $0.007/L, representing a decrease of 36% compared to the SHSS. This reduction is a direct consequence of the increased freshwater productivity resulting from an improvement in thermal performance within the still caused by the magnetic rings. The increase in the daily water production volume, and with the investment cost remaining relatively fixed as the cost of rings is low, the CPL of water reduced for modified solar stills. This illustrates the downward trend in CPL values as the number of magnetic rings increases.

The payback period with percentage reduction for different designs is indicated on Fig 15. The payback period estimated in this study represents a baseline economic payback under the assumed water price, production rate, maintenance conditions, and operating days. Under practical long-term operation conditions, extra and replacement and maintenance expenditures would increase the effective lifecycle cost and extend the actual payback period. The payback period is high and shows an accelerating downward trend with increasing the number of magnet rings. The SHSS recorded the highest payback period of 0.27 years, which then reduced to 0.257 years in the MHS-HFM-5 with a reduction of 5%, 0.22 years in the MHS-HFM-10 case with a decrease of 19%, and 0.20 years in the MHS-HFM-15 case with a 26% decrease, reaching its lowest value of 0.176 years in the MHS-HFM-20 case with a reduction of 35%. The payback period indicates the time required to restore the invested initial cost across the net cash flow produced from the production of freshwater. Any enhancement in thermal efficiency or acceleration in the daily production rate directly decreases this time. In the

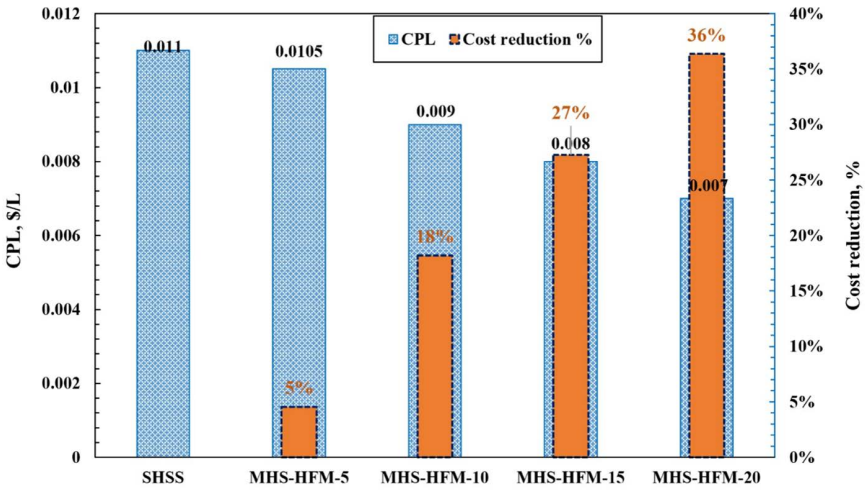

Fig 14. Cost per liter of freshwater and percentage cost reduction relative to SHSS for the studied configurations.

https://doi.org/10.1371/journal.pwat.0000568.g014

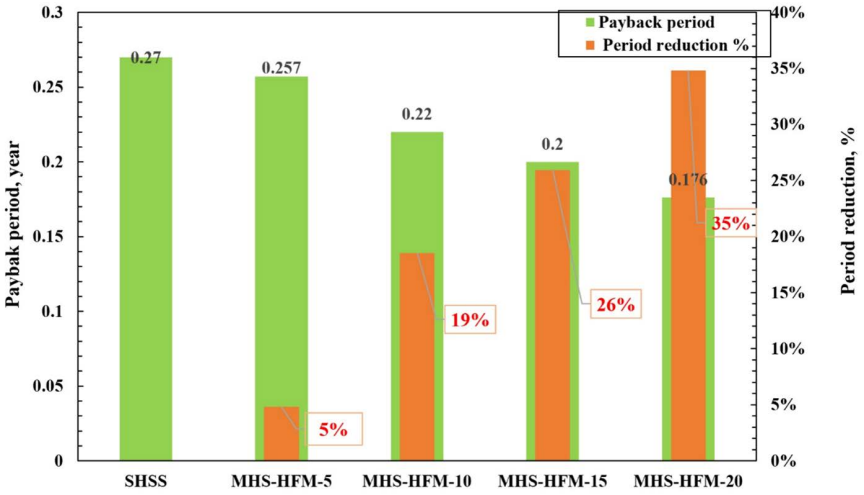

Fig 15. Payback period and percentage reduction relative to SHSS for the different modified configurations under the adopted economic assumptions.

https://doi.org/10.1371/journal.pwat.0000568.g015

modified cases, the magnetic rings gradually increased the temperature of the basin water and hence productivity and thermal performance of the still and extending the effective operating period and improves daily production (from 4.37 L/day to 7.49 L/day, a 71.4% increase). These mechanisms elucidate a strong inverse correlation between increased productivity and decreased payback period. This confirms the effectiveness of the magnetic field not only in the rise of the amount of absorbed solar energy but also in promoting its conversion into usable water production, which decreases financial risk and generates faster cash flow. The acceleration in the enhancement in payback period from 5% to 35% confirms the economic viability of magnetic rings as a magnetic field result in an increase in productivity per unit of investment and thus achieving a faster return on capital cost even with a marginal rise in initial costs from $80 to $90.

The sensitive analysis was carried out to determine the variation of the economic feasibility with local market conditions, including three effective factors: initial material cost, annual maintenance cost, and the selling price of produced freshwater. Table 7 shows the sensitive analysis results for MHS-HFM-20. The material cost was varied by ±10% and ±20% relative to the baseline value to represent possible changes in the costs of the glass cover, basin, insulation, and ferrite magnetic rings. Maintenance costs were estimated at 10% (low case), 15% (base), and 20% (high case) on the adopted cost basis. The local selling price was changed by $0.216/L and $0.324/L around the baseline value of $0.27/L. The results given in Table 7 elucidate that material cost has a direct impact on CPL and payback period. For MHS-HFM-20, the variation in the material cost by ±20% varied the CPL from $0.00581 to $0.00872/L and the payback period from 0.1406 to 0.2117 year. The increase in the maintenance rate from 10% to 20% varied the CPL only from $0.00694 to $0.00759/L and payback period from 0.1760 year to 0.1760, which indicate comparatively lower sensitivity to maintenance expenses. The local price of water exhibited a stronger effect on investment recovery; the decrease in the baseline selling price from $0.27/L to 0.216/L increased the payback period from 0.1760 to 0.2206 year, while increasing it to $0.324/L decreased the payback period to 0.1465 year. While this value has no effect on cost per liter as indicated by equation 11. This analysis confirms that the MHS-HFM-20 maintained the most favorable economic performance across all investigated cases, which reflects the robustness of this configuration under reasonable changes in economic conditions.

Fig 16 indicates the results of final economic analysis used to complete the assessment of economic feasibility using three key financial indicators, including Level Water Cost (LCOW), Benefit-to-Cost Ratio (BCR), and Net Present Value (NPV), each indicator explains a different aspect of investment performance. The LCOW, which represents the true CPL

Table 7. Sensitive analysis results for MHS-HFM-20.

Parameter	Low case	Baseline	High case	CPL, Low ($/L)	CPL, Baseline ($/L)	CPL, High ($/L)	Payback, Low (yr)	Payback, Baseline (yr)	Payback High (yr)
Material cost change	−20%	0%	+20%	0.00581	0.00727	0.00872	0.1406	0.1760	0.2117
Maintenance rate	10%	15%	20%	0.00694	0.00727	0.00759	0.1760	0.1760	0.1760
Water selling price	$0.216/L	$0.270/L	$0.324/L	0.00727	0.00727	0.00727	0.2206	0.1760	0.1465

https://doi.org/10.1371/journal.pwat.0000568.t007

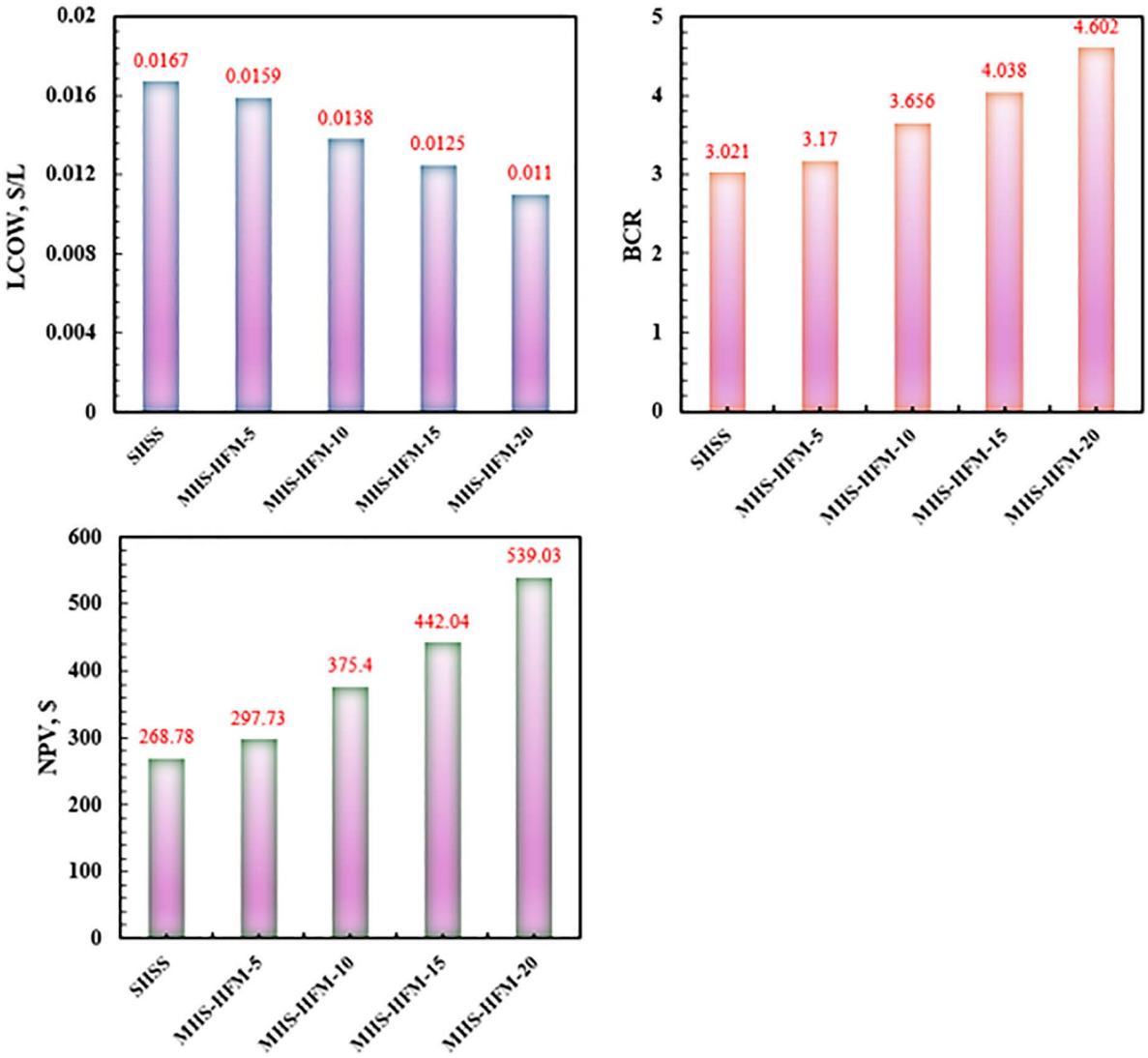

Fig 16. The final economic analysis results via different economic indicators.

https://doi.org/10.1371/journal.pwat.0000568.g016

of freshwater over the lifetime of the solar still, reduced from $0.0167/L in the SHSS to $0.0110/L in the MHS-HFM-20 design, with a reduction of 34.1%. This demonstrates that a higher efficiency in converting the additional intimal cost (only +12.5%) into a clear increase in water productivity of 71.4%, therefore decreasing the real cost per unit of freshwater. The

BCR, which indicates the economic return per dollar invested, rose from 3.021 in the SHSS to 4.602 in the modified still with an increase of 52.3%. This indicates that every dollar spent on the improved solar still produces a return higher than $4.60 over 15 years compared to only $3.0 in the SHSS, thus improving the appeal of the modified design to investors. The NPV, which determines the time value of net profits, nearly doubled from $268.78 in the SHSS to $539.03 in the MHS-HFM-20 design with an increase of 100.5%, reflecting an exceptional profitability even when discounting future cash flows at an interest rate of 12%, which is a strong indicator of robust financial viability. It's worth considering that these economical and performance enhancements are achieved with only a marginal rise in capital cost from $80 to $90, while the daily production increases from 4.37 liters to 7.49 liters. This confirms the efficiency of the magnetic fin technique in improving heat transfer and decreasing heat loss, which maximizes the economic return per unit invested. Consequently, based on the detailed economic indicators the MHS-HFM-20 design is recommended as the best balance between performance and cost for producing freshwater, especially in sunny remote regions with limited resources.

4.3 Environmental analysis results

Fig 17 shows the amount of carbon dioxide (CO_2) mitigated with improvements for different cases. The figure highlights the upward trend in environmental advantages resulting from enhanced solar still performance using magnetic rings. The CO_2 mitigated represents the amount of CO_2 emissions prevented by producing water using solar energy rather than using traditional sources of fossil fuel. The emissions in SHSS decreased by approximately 2.52 tons, while they increased in MHS-HFM-5 to 2.76 tons, with an improvement of 10%. With the addition of further magnetic rings MHS-HFM-10 case, the value increased to 3.33 tons, representing a 32% improvement. This upward trend continued in the MHS-HFM-15 case, achieving 3.83 tons, with a 52% increase. The MHS-HFM-20 achieved the highest amount of CO_2 mitigated, at 4.55 tons, with an increase of 81% compared to the SHSS. This improvement is directly related to the increased temperature of the pond water due to the magnetic rings. The of magnetic rings resulted in a larger amount of fresh water that is replaced compared to what would be produced using traditional, emission-intensive techniques, which illustrates the gradual rise in CO_2 emissions reduction with an increase of magnetic rings number.

Fig 18 illustrates Carbon Credit (in $) and the percentage enhancement for different configurations. The credit value increased proportionally from $36.6 for the SHSS to $40, $48.37, $55.6, for modified stills with 5, 10, and 15 rings, respectively, reaching a maximum value of $66 for the MHS-HFM-20, corresponding to 80% enhancement compared to

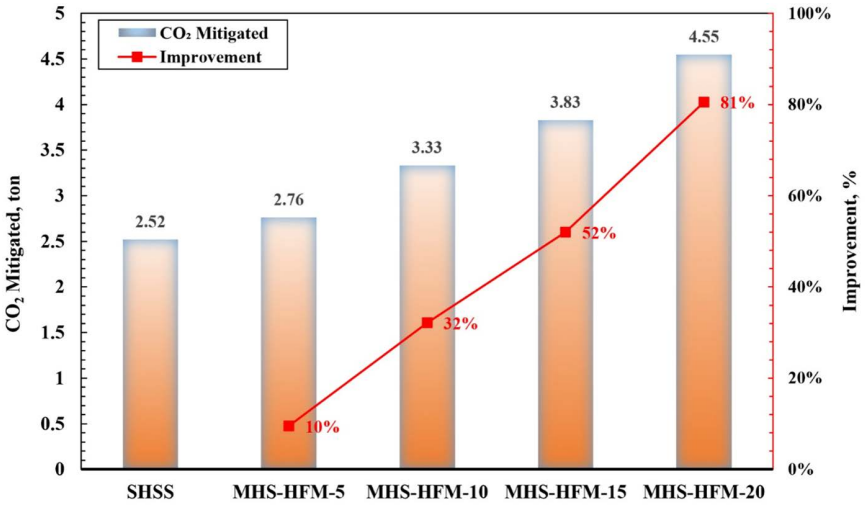

Fig 17. Lifetime net CO_2 mitigation and percentage improvement relative to SHSS for the different solar still configurations.

https://doi.org/10.1371/journal.pwat.0000568.g017

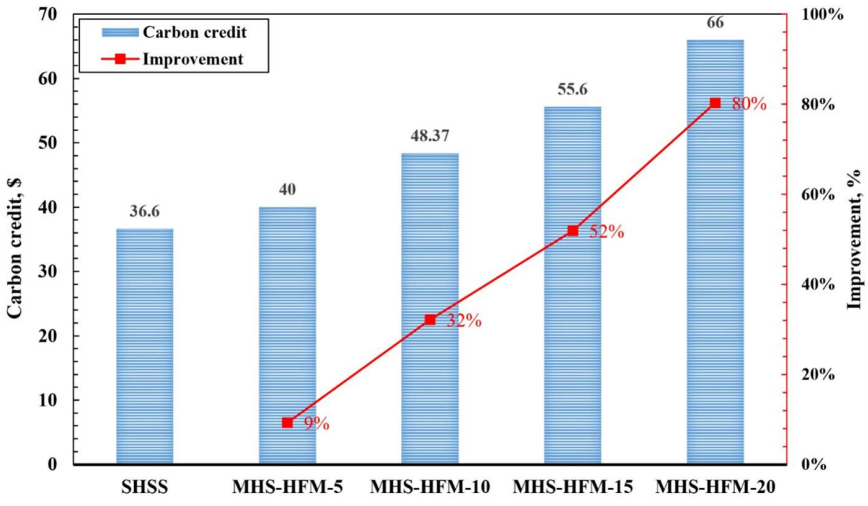

Fig 18. Carbon credit with improvements for standard and modified solar stills.

https://doi.org/10.1371/journal.pwat.0000568.g018

the standard design. The Carbon Credit refers to the financial value gained by the solar still owing to the quantity of CO_2 emissions prevented or decreased using clean solar energy instead of traditional fossil fuel-based energy sources. It is an economic incentive that supports the sustainability of the solar still. The carbon credits can be translated into additional cash revenue trading in global carbon markets, which directly participates in decreasing the actual cost of freshwater production and decreasing the payback period, in addition to its important environmental role in mitigating global warming. The differences in results are directly due to the cumulative impact of the number of magnetic fins on the productivity and thermal performance of the still. Since the carbon credit is determined depending on the total thermal energy utilized, which is directly proportional to the quantity of distilled water, the MHS-HFM-20, with the highest productivity and thermal efficiency, achieved greater savings in energy and hence the greatest decrease in carbon emissions, making it the highest financial value as a carbon credit compared to other designs.

Fig 19 shows the results of the Water-Energy-Carbon Interrelationship Index (WECNI). The WECNI was used to provide an integrated evaluation of the simultaneous impacts of the applied modification on three target outputs of solar still: water production, energy utilization, and environmental benefit. The calculation process involves (1) calculating of freshwater productivity for each case, (2) estimating energy efficiency, (3) estimating the net CO_2 mitigation (4) selecting the SHSS as the reference case and determined a WECNI value for each modified case, (5) Integrated WECNI evaluation. The SHSS had the lowest value for the index of 1, which then significantly increased in MHS-HFM-5 to 1.28 with an increase of 28%. The increase accelerated in the MHS-HFM-10 and MHS-HFM-15 states to 1.75 (75%) and 2.18 (118%), peaking in the MHS-HFM-20 to 2.94 with an enhancement of 194% compared to the baseline state. In the modified solar stills, the gradual rise in basin water temperature is associated with a simultaneous enhancement through all other parameters: increase in daily productivity, energy efficiency, and exergy efficiency along with a reduction in CO_2 emissions. These results reveal that the enhancement in energy conversion efficiency in solar desalination systems not only improves water productivity but also decreases the equivalent reliance on carbon sources, which produces a multiplier impact on overall sustainability. The accelerated enhancement in WECNI with the increasing number of rings from 5 to 20 is due to the uniformity of the magnetic field distribution in a regular grid pattern. This results in a balanced interaction between mechanisms that improve heat transfer, store energy, and decrease thermal resistance, thus enhancing the overall dynamic equilibrium of the solar still. Therefore, the magnetic field increases the basin water temperature by enhancing

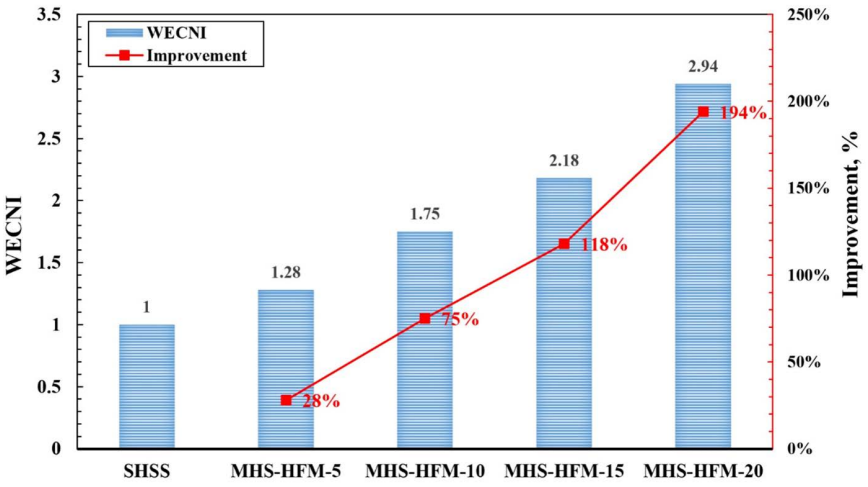

Fig 19. Water–Energy–Carbon Interrelationship Index (WECNI) and corresponding enhancement corresponding to SHSS for different HSS configurations.

https://doi.org/10.1371/journal.pwat.0000568.g019

the physical properties of the saline water and improves the interaction quality between the three components of the indicator. This makes the MHS-HFM-20 an ideal selection for balancing water productivity, energy efficiency, and carbon footprint in sustainable desalination applications.

Table 8 indicates the results of one-way ANOVA and pairwise post-hoc tests analyses. These statistical results offer rigorous quantitative confirmation of the experimental performance trends. The ANOVA analysis shows a high F-value of 18.42 associated with a p-value lower than 0.0001. This elucidates a substantially clear difference between the mean performances of all cases at the standard significance level (α) of 0.05. This rejects the null hypothesis and suggests that the enhancements in magnets are a systematic and reproducible response rather than a random result. The results of Pairwise tests support this holistic finding by meticulously analyzing the differences. The comparison between the SHSS and MHS-HFM-5 yielded a p-value of 0.1425, which exceeds the significance threshold, indicating that the limited enhancement at this low ring number is not statistically significant and may be due to experimental noise or measurement

Table 8. One-way ANOVA and pairwise post-hoc statistical comparison of different HSS configurations at a significance level of α = 0.05.

Results of pairwise post-hoc analysis		
Comparison	**P-Value**	**Significance**
SHSS vs. MHS-HFM-5	0.1425	Not Significant
SHSS vs. MHS-HFM-10	0.0184	Significant
SHSS vs. MHS-HFM-15	0.0006	Highly Significant
SHSS vs. MHS-HFM-20	< 0.0001	Highly Significant
MHS-HFM-15 vs. MHS-HFM-20	0.0211	Significant
ANOVA analysis results		
P-value	< 0.0001	P-value
Significance Level (α)	0.05	Significance Level (α)
F-Statistic	18.42	F-Statistic

https://doi.org/10.1371/journal.pwat.0000568.t008

variability. On the other hand, the p-value sharply reduced with a rise in magnetic distribution, achieving 0.0184 for the MHS-HFM-10 state (statistically significant), then 0.0006 for the MHS-HFM-15 state, and less than 0.0001 for the MHS-HFM-20 state, all classified as highly significant. This scientifically confirms that the cumulative influence of the magnetic field becomes decisive and reliable from 10 rings onwards. Additionally, a direct comparison between the two advanced cases, MHS-HFM-15 vs. MHS-HFM-20, yielded a p-value of 0.0211, which indicates the increase from 15 to 20 rings still represents a clear statistically significant enhancement and not only margin of error or performance saturation.

4.4 Practical implications

From a practical achievement perspective, the applied magnetics rings are still relatively simple, as they don't require any moving components, external power, or complex auxiliary components. The primary required fabrication step is the fixation and positioning of these rings inside the basin depending on the required spacing. Consequently, the increase in the number of rings increases the fabrication complexity, especially for the 20-ring configuration, because more uniform placement is required. Regarding durability, the passive nature of rings is advantageous for long-term utilization; however, long exposure to saline water, salt deposition, and thermal cycling, may influence the surface condition of the rings and any supporting elements. This, consequently, requires periodic cleaning to eliminate salt scaling and deposits from the ring surfaces and basin. In spite of the configurations with a larger number of rings may need slightly more maintenance due to the increase in wetted surfaces, the overall maintenance requirement is still relatively low compared with hybrid or active solar stills. Moreover, long-term outdoor investigation is recommended to identify material degradation and stability, scaling behavior, and maintenance frequency over extended operating periods.

4.5 Comparative study

Table 9 presents a comprehensive comparison between the results of this study and those reported from previous studies employing magnetic fields to enhance the performance of solar stills. The studies provided in Table 9 were performed using different solar still, scales, geometries, operating parameters, climatic conditions, and improvement techniques. Consequently, this comparison reveals the relative performance enhancement rather than a direct comparison of absolute productivity and economic indicators. To enhance the scientific relevance of the comparison, the performance is mainly discussed based on the percentage enhancement of each modified corresponding to its reference still within the same study. The economic indicators, mainly CPL and payback period, relied strongly on specific assumptions, such as system lifetime, material costs, maintenance cost, annual operating period, and interest rate. This comparison reflects a significant distinction and an innovative approach in the application, indicating that the use of permanent magnetic ring fins in the HSS improved productivity by 71.4%, with a decrease in production cost from $0.011/L to $0.0073/L with a 34.1% reduction, and a reduction in the payback period from 0.27 years to 0.176 years, only 64 days. These results were comparable to previous studies, such as [35], which used magnetic fins with steel coils and a nano-silver coating, achieved a productivity increase of 19.7–60.3% at a cost of $0.015/L. Study [48], using rectangular fins, PCM, and a magnetic field, improved productivity to 99.81% at a cost of $0.035/L. Study [49], using a tubular still, achieved a 204% increase in productivity at a cost of $0.009/L, and study [50], using an axial cylindrical magnetic field, achieved a 65.36% improvement in productivity. This study is distinguished by several parameter compared to other previous studies: First, the use of different numbers of rings, 5, 10, 15, 20, with different spacing (150, 120, 90, 60 mm respectively) to achieve an optimum distribution of the magnetic field within the basin, something that has not been previously studied. Second, the use of permanent magnets only without any other modifications such as used in other studies, which drastically decreases complexity and costs. Third, achieving the best balance between performance and production cost. The obtained results surpass most previous studies in terms of the low CPL, $0.0073 compared to $0.009 − $0.035 in other studies, with a payback period of 64 days compared to 103 days in study [48] and 2.8 years in study [35]. Fourth, the design of used HSS is simple, and it is easy to construct and more applicable on a large scale, unlike the complexities related to using

Table 9. Baseline-normalized technical comparison of the present magnetic ring HSS with previous studies.

SS design	Modifications	Performance improvement	Ref.
HSS	Magnetic fins, stainless-steel coils, and AgNps coating	The Productivity and energy efficiency increased by 19.7–60.3% and 19.5–59.4%. The production cost was reduced to 0.015 $/L and a payback period reduced to 2.8 years.	[35]
Double slope	PCM, rectangular fins, and magnetic field	Water yield, energy and exergy efficiency increased to 99.81%, 67.1 and 1.97% The CPL and payback period reduced to 0.035$/L and 103 days with CO_2 mitigation amount of 5.94 tons/y.	[51]
Tubular	Magnetic field application, PCM + Ag, and vertical wick	Water yield increased by 204% and thermal efficiency increased by 60.6% the production cost reduced to 0.009 $/L.	[52]
HSS	Axial magnetic cylindrical	Water yield improved by 65.36%, energy efficiency improved by 64.12%, The cost and payback period decreased 10.14–37.80% and 36.36–72.73%.	[53]
Stepped SS	A permanent magnetic field with PCM	Water yield improved by 131.1%, with energy efficiency of 15.7%	[54]
Multi-slope SS	Thermoelectric cover cooling and magnetic stirrer	Water yield improved by 55.5% using magnetic stirrer, and by 1431.4% using both techniques. The energy and exergy efficiency were 28% and 1.67%, and the CPL was 0.081 $.	[55]
Stepped solar still	Hybrid NPCM under constant magnetic field	Water yield improved by 98% and thermal efficiency was 13.6%.	[56]
Conical solar	Disc magnets with external truncated reflectors	The maximum water yield was 9.46 L/m^2, thermal efficiency was 72.975, and exergy efficiency improved by 331.30%. The CPL reduced to $0.0076 and payback period decreased to 1.51 months.	[57]
Tubular	Permanent magnets, nanoparticles, reflector	Water yield improved by 56.5-70%, and thermal efficiency was 23–54%, exergy efficiency 128–152% with CPL of $0.0117.	[58]
HSS	Magnetic rings	Productivity, energy and exergy efficiency improved by 72%, 65 and 172%. The CPL and payback period reduced to $0.007/L and 0.176 year with CO2 mitigation amount of 4.55 tons/y.	Current study

https://doi.org/10.1371/journal.pwat.0000568.t009

nanoparticles, PCM, or hybrid modifications. The findings of this study confirm that simple magnetic modification can achieve exceptional enhancement in productivity and thermal performance without significant additional costs.

5. Conclusion

The outcomes of this work demonstrate that the use of magnetic ring fins in the hemispherical solar still is an effective method for enhancing its productivity and thermal performance. A comparison between the traditional solar still and the modified stills revealed that the increase in the number of magnetic rings, while reducing their spacing, significantly enhanced heat transfer inside the still owing to the increased effective surface area and promoted heat exchange between the water and basin surface. This, in turn, leads to an increase in basin water temperature from 45°C to 50.5°C, which accelerates the evaporation rate. Among the studied cases, the configuration with 20-ring arrangement achieved the best overall performance. The freshwater productivity increased from 4.37 L/m²·day to 7.50 L/m²·day in the modified still, representing an enhancement of 72%. The modified stills converted a larger portion of the available solar energy into useful evaporative energy and indicated a substantial enhancement in thermodynamic performance, as the thermal efficiency and exergy efficiency increased from 27% to 56% and 1.31% to 3.56%, respectively. The economic analysis further confirmed that the additional cost related to the magnetic rings was small, with CPL of $0.011/L, compared to the gain in freshwater production and a lower payback period of 0.176 year. Regarding environmental analysis, the obtained results revealed a greater potential for CO_2 mitigation, with reduced CO_2 emissions increasing from 2.52 tons to 4.55 tons thanks to the increased dependence on solar energy for water production. Collectively, integrating magnetic rings gives a promising balance between freshwater production, thermal performance, economic feasibility, and environmental benefit. Therefore, the study recommends the 20-rings design for small-scale and decentralized desalination systems in regions with high solar irradiance.

The limitations/future work

Despite the promising findings of this study, some limitations are required to consider in future studies. The present experimental design can't isolate the magnetic contribution from the improvement resulting from additional heat transfer surface area. Furthermore, the increase in the number of rings simultaneously reduces the spacing between rings and increases the total exposed surface area. Consequently, ring number, surface area, spacing, and magnetic field distribution are coupled variables in this work and should not be interpreted as independent variables. Studying the effect of non-magnetic surface with the same characteristics of rings wasn't considered to indicate the incremental magnetic field contribution to be isolated from the traditional fin induced heat transfer improvement. The precipitation of salt on the magnetic rings and basin can result in a decrease in effective heat transfer area, an additional thermal resistance, and partially shield the ring surfaces from direct contact with saline water. Furthermore, salt carryover on the glass cover can decrease optical transmittance and may adversely impact solar transmission and condensation. Therefore, the following recommendations should be addressed in future studies:

- Long-term experiments should be considered to evaluate salt scaling on the magnetic rings, basin, and glass-cover fouling, and the resulting degradation in productivity thermal and performance.
- Studying distribution geometry of rings to identify whether extra performance gains can be achieved without the increase in the manufacture and maintenance requirements.
- Long-duration investigation to achieve realistic cleaning frequency, corrosion behavior, scaling rate, replacement intervals, magnetic-field degradation, and their corresponding lifecycle cost.
- Further mechanistic evaluation should include a geometrically identical non-magnetic control manufactured from a material having the same thermophysical properties and dimensions as close as possible to those of the magnetic rings.

Abbreviations

Symbol/ abbreviation	Definition	Unit
BCR	Benefit-cost ratio	–
CPL	Cost per liter of produced freshwater	$ L^{-1}
HSS	Hemispherical solar still	–
LCOW	Levelized cost of water	$ L^{-1}
NPV	Net present value	$
PCM	Phase change material	–
WECNI	Water-Energy-Carbon Interrelationship Index	–
A_b	Basin area	m^2
E_{in}	Energy input to the solar still	J or W
E_{out}	Useful energy output	J or W
hfg	Latent heat of vaporization of water	$J\ kg^{-1}$
I	Solar irradiance incident on the still	$W\ m^{-2}$
m_f	Freshwater mass	kg
MA	Annual freshwater yield	$L\ year^{-1}$
Nday	Number of operating days per year	$day\ year^{-1}$
η_{en}	Energy efficiency	%
η_{ex}	Exergy efficiency	%
Ta	Ambient air temperature	°C or K
Tw	Basin-water temperature	°C or K
Tgi	Inner glass-cover temperature	°C

Symbol/ abbreviation	Definition	Unit
Tsun	Effective temperature of the sun	K
TAC	Total annual cost	$ $year^{-1}$
AMC	Annual maintenance cost	$ $year^{-1}$
ASC	Annual salvage value term	$ $year^{-1}$
P	Initial capital cost of the solar still	$
CF	Annual cash flow	$ $year^{-1}$
Mv	Market value of produced freshwater	$ L^{-1}
i	Interest rate	–
CRF	Capital recovery factor	–
O&MC	Operating and maintenance cost	$ $year^{-1}$
NM_{CO2}	Net amount of CO_2 mitigation	ton CO_2
CC_{CO2}	Carbon credit associated with avoided CO_2 emissions	$
Conv	Convective heat transfer	W m^{-2}
Rad	Radiative heat transfer	W m^{-2}

https://doi.org/10.1371/journal.pwat.0000568.t010

Acknowledgments

This project is sponsored by Prince Sattam bin Abdulaziz University (PSAU) as part of funding for its PSAU Global South Partnership (GSP) project number PSAU-RDEP-2025-0157.

Author contributions

Conceptualization: Abdekader S. Abdullah, Suha A. Mohammed, İsmail Solmaz, Hamada Mohamed Abdelmotalib.

Data curation: İsmail Solmaz.

Formal analysis: Eyad Zaky, khaled harby.

Investigation: Abdekader S. Abdullah, khaled harby.

Methodology: khaled harby.

Resources: Eyad Zaky.

Software: Abdekader S. Abdullah.

Supervision: Abdekader S. Abdullah, Sengottain Shanmugan.

Visualization: Sengottain Shanmugan.

Writing – original draft: Eyad Zaky, Sengottain Shanmugan, Hamada Mohamed Abdelmotalib.

Writing – review & editing: Suha A. Mohammed, İsmail Solmaz, Hamada Mohamed Abdelmotalib.

References

1. Harby K, Elazab MA, Daoush WM, Alanezi A. Optimizing the productivity of solar distillers using nanoparticle-coated multi-sand basins filled with different contents of waste aluminum filings. Int Commun Heat Mass Transf. 2026;176:111319. https://doi.org/10.1016/j.icheatmasstransfer.2026.111319
2. Attia MEH, Abdelgaied M, Amin M, Harby K. Experimental investigation of a novel egg steel trays covered with wick materials effects on the performance of conical solar distillers: A 4E analysis and multi-objective optimization. J Water Process Eng. 2024;68:106601. https://doi.org/10.1016/j.jwpe.2024.106601
3. Saito K, Irie M, Zaitsu S, Sakai H, Hayashi H, Tanioka A. Power generation with salinity gradient by pressure retarded osmosis using concentrated brine from SWRO system and treated sewage as pure water. Desalin Water Treat. 2012;41(1–3):114–21. https://doi.org/10.1080/19443994.2012.664696

4. Harby K, Alsaman AS, Ali ES. Innovative and efficient integrations of desalination plants coupled absorption, adsorption, and humidification-dehumidification desalination units employing external heat recovery techniques. Energy Convers Manag. 2024;314:118667. https://doi.org/10.1016/j.enconman.2024.118667
5. Choi J, Oh Y, Chae S, Hong S. Membrane capacitive deionization-reverse electrodialysis hybrid system for improving energy efficiency of reverse osmosis seawater desalination. Desalination. 2019;462:19–28. https://doi.org/10.1016/j.desal.2019.04.003
6. Alsaman AS, Ali ES, Harby K, Ben-Mansour R, Mansour RB. Techno-economic evaluation of novel combinations of reverse osmosis with absorption and HDH desalination systems for energy utilization and sustainability. Sustain Energy Technol Assess. 2025;81:104451. https://doi.org/10.1016/j.seta.2025.104451
7. Ali ES, Alsaman AS, Harby K, Alanezi A, Mansour RB, Ben-Mansour R. Evaluating performance of desalination plant integrating absorption cycle, humidification-dehumidification system, and internal heat recovery process for sustainable water production. Int Commun Heat Mass Transf. 2026;170:110041. https://doi.org/10.1016/j.icheatmasstransfer.2025.110041
8. Lv H, Wang Y, Wu L, Hu Y. Numerical simulation and optimization of the flash chamber for multi-stage flash seawater desalination. Desalination. 2019;465:69–78. https://doi.org/10.1016/j.desal.2019.04.032
9. Abdullah AS, Rezk H, Omara ZM, Harby K. Comprehensive evaluation of hybrid solar distillation systems using spiral base copper fins, waste copper shavings-enhanced PCM, and external condenser coupled with PV-thermoelectric.
10. Attia MEH, Harby K, Bedairi BH, Abdelgaied M. An experimental study on increasing the productivity of novel conical solar distillers with flat and egg steel trays basins: Energy, exergy, and exergo-economic evaluation. Solar Energy. 2025;287:113258. https://doi.org/10.1016/j.solener.2025.113258
11. Attia MEH, Harby K, Bedairi BH, Abdelgaied M. Performance optimization and 4E evaluation of a conical solar still using welded steel mesh as a secondary porous absorber: Impact of varying hole sizes. Solar Energy Mater Solar Cells. 2025;283:113463. https://doi.org/10.1016/j.solmat.2025.113463
12. Abed AF, Alshukri MJ, Hachim DM. Improving solar still performance via the integration of nanoparticle-enhanced phase change materials: A novel pyramid-shaped design with a numerical simulation approach. J Energy Storage. 2024;97:112980. https://doi.org/10.1016/j.est.2024.112980
13. Adam A, Saffaj N, Mamouni R. Sustainable solar still system coupled with renewable power for industrial wastewater recycling: A review. Mater Today: Proc. 2023. https://doi.org/10.1016/j.matpr.2023.03.416
14. Handawy MKM, Harby K, Abdel-Aziz MM, Abdelmotalib HM. Feedwater preheating and water inlet techniques in solar distillation systems as effective and economic solutions for sustainable freshwater supply: A comprehensive review of recent developments. Int Commun Heat Mass Transf. 2026;175:111049. https://doi.org/10.1016/j.icheatmasstransfer.2026.111049
15. Bacha HB, Abdullah AS, Abdelgaied M, Harby K. Enhancing the thermal performance of hemispherical solar distillers using an innovative, sophisticated combination of enhancements. Solar Energy Mater Solar Cells. 2026;299:114231. https://doi.org/10.1016/j.solmat.2026.114231
16. Dhivagar R, Jidhesh P, Kannan KG, Kim SC. Thermo-economic and environmental assessment of a sustainable trigeneration double slope solar still integrated with a single-side mounted photovoltaic panel and electrical heating element. Sep Purif Technol. 2026;380:135226. https://doi.org/10.1016/j.seppur.2025.135226
17. Deep R, Sharma N, Prabhakar V. Performance, environmental, sustainability and water quality assessment of solar water desalination systems utilizing recycled thermal energy storage materials. Solar Energy Mater Solar Cells. 2026;304:114440. https://doi.org/10.1016/j.solmat.2026.114440
18. Abdullah AS, Rezk H, Abdelmotalib HM, Harby K. Innovative deep learning model for optimizing solar distiller performance using recycled thermal conductive materials enhanced PCM: Effective, economical, and sustainable techniques. Solar Energy Mater Solar Cells. 2026;307:114578. https://doi.org/10.1016/j.solmat.2026.114578
19. Sharma N, Mahala T. Synergistic enhancement of solar still performance via Eco-friendly packed bed heat storage and natural cloth materials. Process Saf Environ Prot. 2026;209:108624. https://doi.org/10.1016/j.psep.2026.108624
20. Younis O, Hussein AK, Attia MEH, Rashid FL, Kolsi L, Biswal U, et al. Hemispherical solar still: Recent advances and development. Energy Rep. 2022;8:8236–58. https://doi.org/10.1016/j.egyr.2022.06.037
21. Jodah FT, Alawee WH, Dhahad HA, Omara Z. Evaluating the performance of spherical, hemispherical, and tubular solar stills with various configurations - A detailed review. Proc Inst Mech Eng A: J Power Energy. 2024;238(7):1261–96. https://doi.org/10.1177/09576509241266284
22. Arunkumar T, Raj K, Kabeel A-E, Lee SJ. Effects of solar geometry and operation period on stability of solar desalination systems: A review. Environ Sci Pollut Res Int. 2021;28(46):65014–32. https://doi.org/10.1007/s11356-021-16566-8 PMID: 34611805
23. Harby K, Elazab MA, Amin M. Synergistic thermal storage and nanofluid-assisted solar heating for performance enhancement of a hemispherical solar still. Appl Therm Eng. 2026;303:132546. https://doi.org/10.1016/j.applthermaleng.2026.132546
24. Muftah AliF, Alghoul MA, Fudholi A, Abdul-Majeed MM, Sopian K. Factors affecting basin type solar still productivity: A detailed review. Renew Sustain Energy Rev. 2014;32:430–47. https://doi.org/10.1016/j.rser.2013.12.052
25. Harby K, Handawy MK, Abdelmotalib HM, Daoush WM. Hemispherical solar stills integrated with wavy, circular honeycomb-shaped absorber, nanoparticles-coated recycled cups, and copper shavings-enhanced PCM: Comprehensive 4E and heat transfer evaluation. Solar Energy Mater Solar Cells. 2026;307:114581. https://doi.org/10.1016/j.solmat.2026.114581
26. Alqsair UF, Joseph A, Abdullah AS, Sharshir SW. High-efficiency desalination of hemispherical solar still incorporating dish collector, hanging wick, nanofluids, back reflector, and external condenser: A 4E perspective. Appl Therm Eng. 2026;288:129550. https://doi.org/10.1016/j.applthermaleng.2025.129550

27. Abed AF, Alshukri MJ, Alsayah AM, Al Takash A, Murr R, Khaled M. Performance enhancement of hemispherical solar stills using a rotating Wick drum and glass cover water-film cooling. Int Commun Heat Mass Transf. 2026;174:110907. https://doi.org/10.1016/j.icheatmasstransfer.2026.110907
28. Prabhu B, Attia MEH, Abdel-Aziz MM. Hybrid heat-transfer enhancement in hemispherical solar stills employing boules scrubber metallic inox and copper oxide nanoparticles. Sep Purif Technol. 2026;383:136161. https://doi.org/10.1016/j.seppur.2025.136161
29. Harby K, Abdelmotalib HM, Abdelgaied M, Amin M, Hussein Farh HM, Al-Shamma'a AA. AI-driven machine learning and experimental optimization for sustainable solar distillers using recycled stainless-steel shavings-enhanced PCM and ag-NPs-coated recycled cans. Sep Purif Technol. 2026;392:137158. https://doi.org/10.1016/j.seppur.2026.137158
30. Abdelaziz GB, Eldafrawy MM, Dahab MA, Abdelgaleel M, Marie HS, Habba MIA, et al. Enhancing water productivity in hemispherical solar stills: Integration of evacuated tube collectors and response surface methodology analysis. Int Commun Heat Mass Transf. 2026;172:110427. https://doi.org/10.1016/j.icheatmasstransfer.2025.110427
31. Abdel-Aziz MM, Kabeel AE, Attia MEH. Sustainable solar desalination via surface tension manipulation: Experimental analysis of charcoal powder in hemispherical stills. Int J Heat Fluid Flow. 2026;117:110150. https://doi.org/10.1016/j.ijheatfluidflow.2025.110150
32. Harby K, Abdelmotalib HM, Handawy MK, Almetwally EM. Performance improvement of hemispherical solar stills integrating low-cost recycled copper shavings enhanced-PCM and waste aluminum cans: experimental and predictive modeling with multi-layer perceptron AI. Sep Purif Technol. 2026;394:137560. https://doi.org/10.1016/j.seppur.2026.137560
33. Alahmadi YH, Attia MEH, Harby K, Abdelgaied M. Optimization and comparative study of hemispherical solar stills using welded wire mesh as a secondary porous absorber– Part II: Impact of varying positions in water basins. Solar Energy Mater Solar Cells. 2025;290:113688. https://doi.org/10.1016/j.solmat.2025.113688
34. Attia MEH, Harby K, Amin M, Abdelgaied M. Improving the performance of hemispherical solar stills using innovative copper tubes arranged in a honeycomb structure with natural sponges coated with nanoparticles. Appl Therm Eng. 2025;269:126130. https://doi.org/10.1016/j.applthermaleng.2025.126130
35. Harby K, Aboelmaaref MM, Hussein Farh HM, Mekhilef S, Al-Shamma'a AA. Comprehensive 4E analysis of cost-effective, integrated hemispherical solar stills with nano-coated stainless-steel spherical-coils enhanced with magnetic round fins. Int Commun Heat Mass Transfer. 2026;173:110770. https://doi.org/10.1016/j.icheatmasstransfer.2026.110770
36. Essa FA, Basem A, Shaaban SM, Mohammed SA, Alawee WH, Abdullah AS, et al. Synergistic enhancement of hemispherical solar stills: magnetic field application, vertical Wick integration, and nano-enhanced PCM. Sep Purif Technol. 2026;380:135321. https://doi.org/10.1016/j.seppur.2025.135321
37. Attia MEH, Harby K, Benghanem M, Abdelgaied M, Alqurashi HF. Productivity enhancement of hemispherical solar distillers with the use of nanoparticle-coated recycled metal cans arranged in a honeycomb pattern and magnetic fins. Int Commun Heat Mass Transf. 2026;172:110691. https://doi.org/10.1016/j.icheatmasstransfer.2026.110691
38. Holysz L, Szczes A, Chibowski E. Effects of a static magnetic field on water and electrolyte solutions. J Colloid Interface Sci. 2007;316(2):996–1002. https://doi.org/10.1016/j.jcis.2007.08.026 PMID: 17897662
39. Cai R, Yang H, He J, Zhu W. The effects of magnetic fields on water molecular hydrogen bonds. J Mol Struct. 2009;938:15–9. https://doi.org/10.1016/j.molstruc.2009.08.037
40. Kitazawa K, Ikezoe Y, Uetake H, Hirota N. Magnetic field effects on water, air and powders. Phys B: Condens Matter. 2001;294–295:709–14. https://doi.org/10.1016/s0921-4526(00)00749-3
41. Nakagawa J, Hirota N, Kitazawa K, Shoda M. Magnetic field enhancement of water vaporization. J Appl Phys. 1999;86:2923–5. https://doi.org/10.1063/1.371144
42. Zhou KX, Lu GW, Zhou QC, Song JH, Jiang ST, Xia HR. Monte Carlo simulation of liquid water in a magnetic field. J Appl Phys. 2000;88:1802–5. https://doi.org/10.1063/1.1305324
43. Iwasaka M, Ueno S. Structure of water molecules under 14 T magnetic field. J Appl Phys. 1998;83:6459–61. https://doi.org/10.1063/1.367737
44. Szcześ A, Chibowski E, Hołysz L, Rafalski P. Effects of static magnetic field on water at kinetic condition. Chem Eng Process: Process Intensif. 2011;50(1):124–7. https://doi.org/10.1016/j.cep.2010.12.005
45. Alahmadi YH, Attia MEH, Abdelgaied M, Harby K, Bedairi BH. Comparative experimental analysis of innovative extended magnetic poles effects on the performance of conical solar distillers: Multi-objective optimization and 3E analysis. Solar Energy. 2025;292:113448. https://doi.org/10.1016/j.solener.2025.113448
46. Harby K, Abdel-Aziz MM, Al Ani H, Daoush WM. Thermo-magnetic enhancement of a hemispherical solar still with ferrite fins. Appl Therm Eng. 2026;299:131215. https://doi.org/10.1016/j.applthermaleng.2026.131215
47. Holman JP, Gajda WJ. Experimental methods for engineers. McGraw-Hill; 1978.
48. Abdullah AS, Rezk H, Omara ZM, Harby K, Kazem HA. Enhancing thermal storage and performance of hemispherical solar stills using new proposed spiral base copper fins within phase change material and corrugated reflectors: Comprehensive evaluation. J Energy Storage. 2026;172:123001. https://doi.org/10.1016/j.est.2026.123001

49. Handawy MK, Attia MEH, Khelifa A, Harby K, Abdelgaied M, Abdelmotalib HM. Artificial intelligence–driven CFD simulation and thermal optimization of a finned bi-fluid PVT collector. Int Commun Heat Mass Transf. 2026;176:111434. https://doi.org/10.1016/j.icheatmasstransfer.2026.111434
50. Dwivedi VK, Tiwari GN. Thermal modeling and carbon credit earned of a double slope passive solar still. Desalin Water Treat. 2010;13(1–3):400–10. https://doi.org/10.5004/dwt.2010.856
51. Shabestari ST, Esmaeili MS, Kasaeian G, Kasaeian A. Comprehensive evaluation of a portable double-slope solar still equipped with rectangular fins, PCM, and magnetic field: Energy, exergy, economic and environmental analysis (4E). Energy. 2026;351:140574. https://doi.org/10.1016/j.energy.2026.140574
52. Shaaban SM, Basem A, Mohammed SA, Alawee WH, Aldabesh A, Abdullah AS, et al. Performance enhancement of tubular solar still through magnetic field integration and vertical wick Configuration: Experimental investigation of multi-enhancement strategies. Case Stud Therm Eng. 2025;74:106758. https://doi.org/10.1016/j.csite.2025.106758
53. Attia MEH, Harby K, Bedairi BH, Abdelgaied M. Improving the performance of hemispherical solar stills using four axial magnetic cylindrical magnets: Innovative configurations for optimizing magnetic field distribution. Appl Therm Eng. 2025;266:125773. https://doi.org/10.1016/j.applthermaleng.2025.125773
54. Toosi SSA, Goshayeshi HR, Zahmatkesh I, Chaer I, Salahshour S, Toghraie D. Effect of rectangular, triangular, and semi-circular hybrid nano phase change material chambers under permanent magnetic field on the stepped solar still efficiency: An experimental study. Case Stud Therm Eng. 2024;59:104451. https://doi.org/10.1016/j.csite.2024.104451
55. Rabishokr K, Daghigh R. A portable solar still's productivity boost combining a magnetic stirrer and thermoelectric. Desalination. 2023;549:116340. https://doi.org/10.1016/j.desal.2022.116340
56. Adibi Toosi SS, Goshayeshi HR, Zahmatkesh I, Nejati V. Experimental assessment of new designed stepped solar still with Fe3O4 + graphene oxide + paraffin as nanofluid under constant magnetic field. J Energy Storage. 2023;62:106795. https://doi.org/10.1016/j.est.2023.106795
57. Amin M, Attia MEH, Benghanem M, Handawy MK, Harby K, Abdelgaied M. 4E assessment and production optimization of conical solar distillers: Investigating the dual effect of magnetic field distribution of disc magnets with external truncated reflectors. Int Commun Heat Mass Transf. 2026;172:110558. https://doi.org/10.1016/j.icheatmasstransfer.2026.110558
58. El-Fakharany MK, El-Mahs AN, Abd-ElAziz MA, Qasim KF, Sharaf MA, Marzouk SA. Sustainable freshwater production using nanoparticles, permanent magnets, and reflective surfaces in tubular solar stills. Sustain Energy Technol Assess. 2026;86:104850. https://doi.org/10.1016/j.seta.2026.104850